TECHNICAL MEMORANDUM

X-566

SUBSONIC AERODYNAMIC CHARACTERISTICS OF DISK RE-ENTRY CONFIGURATIONS WITH ELLIPTIC CROSS SECTIONS AND THICKNESS-DIAMETER RATIOS OF 0.225 AND 0.325

By Fred A. Demele and Jack J. Brownson

Ames Research Center
Moffett Field, Calif.

NATIONAL AERONAUTICS AND SPACE ADMINISTRATION

WASHINGTON

May 1961

1S

UNCLASSIFIED

CONFIDENTIAL

NATIONAL AERONAUTICS AND SPACE ADMINISTRATION

TECHNICAL MEMORANDUM X-566

SUBSONIC AERODYNAMIC CHARACTERISTICS OF DISK RE-ENTRY CONFIGURATIONS WITH ELLIPTIC CROSS SECTIONS AND THICKNESS-DIAMETER RATIOS OF 0.225 AND 0.325*

By Fred A. Demele and Jack J. Brownson

SUMMARY

An investigation has been made to determine the longitudinal and lateral-directional aerodynamic characteristics of two disk-shaped re-entry configurations employing trailing-edge control surfaces, vertical stabilizing surfaces, and canopies. The models had elliptic profiles with maximum thickness-diameter ratios of 0.225 and 0.325. The tests were conducted to maximum angles of attack of 28° and angles of sideslip of 19° over a range of Mach numbers from 0.25 to 0.90 at a Reynolds number of 3.3×10^6 and at Reynolds numbers to 16×10^6 at a Mach number of 0.25.

It was found that with the moment center located at 40 percent of the diameter, both model configurations were longitudinally stable at low speeds. At Mach numbers from 0.80 to 0.90, the models exhibited varying degrees of instability up to the region near maximum lift, wherein a stable trend in the pitching moments normally occurred. Deflection of the trailing-edge flaps resulted in practically no adverse effects on the lift-drag ratios at low speeds and was an effective means for trim change. At low speeds and for a lift coefficient of about 0.4, the trim lift-drag ratio for the model having a thickness-diameter ratio of 0.225 was 6 and that for the thicker model was almost 5. Both models were directionally stable and exhibited positive effective dihedral throughout the Mach number range.

*Title, Unclassified

INTRODUCTION

General interest in manned space flight has provided a stimulus for the investigation of shapes which appear to be attractive for application to re-entry vehicles. Such vehicles can be classed as either nonlifting or lifting. Nonlifting types, such as used in Project Mercury, have certain advantages which include structural simplicity, no requirement for an elaborate flight-control system, ease of mating the booster, and short exposure times to high heating rates during entry. Advantages of lifting types, by comparison, include lower peak heating rates and decelerations, the possibility for a conventional horizontal landing, and the ability to maneuver, thus providing control over longitudinal and lateral range and a deeper entry corridor on return from planetary or lunar missions (see, e.g., ref. 1).

A lifting shape which appears attractive in terms of the foregoing considerations is a thick disk. At high attitudes, the weight-to-drag ratio is low and the radius of curvature of the surface exposed to the airstream is large, a combination of parameters which results in reduced convective heating rates (see, e.g., ref. 2). As shown in reference 3, the low-speed lift-drag ratios associated with this type of shape appear sufficiently high to permit a conventional horizontal landing. However, the results of the investigation reported in reference 3, which was made to determine the subsonic aerodynamic characteristics of basic disk shapes having elliptic cross sections and thickness-diameter ratios from 0.225 to 0.425, showed that the basic disk shape is longitudinally unstable at attitudes associated with conventional horizontal landing.

One method of providing stability has been investigated at low speeds and reported in reference 4. This involved the addition of horizontal fins with end plates to a disk having biconvex cross sections with a thickness-diameter ratio of 0.29. The horizontal-fin and end-plate arrangement was also incorporated in a disk model having elliptic cross sections with a thickness-diameter ratio of 0.367 and the resulting configuration was tested at transonic speeds (ref. 5) and at supersonic speeds (ref. 6). The method of providing longitudinal stability used in the present investigation involved the addition of trailing-edge control surfaces to basic disk shapes.

The investigation reported herein was undertaken to determine the longitudinal and lateral-directional aerodynamic characteristics of disk configurations employing trailing-edge control surfaces, vertical surfaces on the body, and canopies. The models had elliptic cross sections with thickness-diameter ratios of 0.225 and 0.325. The tests were conducted in the Ames 12-Foot Pressure Wind Tunnel over a Mach number range from 0.25 to 0.90 at a Reynolds number of 3.3×10^6, and at Reynolds numbers to 16×10^6 at a Mach number of 0.25. Data were obtained for

angles of attack to 28° and for angles of sideslip to 19°. The results of an investigation of the aerodynamic characteristics of these two models at supersonic speeds are presented in reference 7.

NOTATION

The data on the longitudinal characteristics are referred to the wind axes, and the data on the lateral-directional characteristics are referred to the body axes. The origin of the axes, or moment center, was located 40 percent of the diameter back from the nose in the chord plane of the models. The coefficients are based on plan-form area, including flap area when flaps are incorporated on the model.

C_D drag coefficient, $\frac{\text{drag}}{qS}$

C_L lift coefficient, $\frac{\text{lift}}{qS}$

C_m pitching-moment coefficient, $\frac{\text{pitching moment}}{qSd}$

C_n yawing-moment coefficient, $\frac{\text{yawing moment}}{qSd}$

C_l rolling-moment coefficient, $\frac{\text{rolling moment}}{qSd}$

C_Y side-force coefficient, $\frac{\text{side force}}{qS}$

d diameter of model

$\frac{L}{D}$ lift-drag ratio

M free-stream Mach number

q free-stream dynamic pressure

R Reynolds number, based on model diameter

r radial distance from center of model

S plan-form area of model

$\frac{t}{d}$ maximum thickness to diameter ratio

y	vertical distance from the chord plane
α	angle of attack, measured with respect to the chord plane
β	angle of sideslip
δ	deflection angle of longitudinal control surfaces, positive downward (see fig. 2(a))
$\left(\frac{dC_L}{d\alpha}\right)_{\alpha=0^\circ \text{ to } 5^\circ}$	lift-curve slope in the vicinity of $\alpha = 0^\circ$ to 5°, per deg
$\left(\frac{dC_m}{dC_L}\right)_{C_L=0 \text{ to } 0.1}$	pitching-moment-curve slope in the vicinity of $C_L = 0$ to 0.1
C_{Y_β}, C_{l_β}, C_{n_β}	derivatives with respect to β, per deg

Subscript

max	maximum

MODELS

Two disk models with elliptic profiles were tested in this investigation (see fig. 1). The models had diameters of 2 feet and maximum thickness-diameter ratios of 0.225 and 0.325. The model with a thickness-diameter ratio of 0.225 incorporated a negative 2.5-percent semielliptic mean-line camber. The other model was symmetrical about the chord plane. The model shapes were generated by revolving about the minor axis the elliptical sections described in table I. The model configurations incorporated canopies, twin vertical surfaces, and longitudinal-control surfaces. One canopy, referred to as the large canopy, had a spherical shape and the other, referred to as the small canopy, was a more streamlined shape. The two vertical surfaces had a combined area of about 11 percent of the disk area. Two sets of longitudinal-control surfaces, or flaps, were utilized which had total areas of 20 and 25 percent of the disk area, respectively. Additional model details are shown in figures 2 and 3.

The models, which were supported by a 2.5-inch-diameter sting, enclosed a six-component strain-gage balance which was used to measure the forces and moments. A cylindrical fairing was provided at the base of the models to enclose the sting within the body (see figs. 1, 2, and 3). Base pressures were measured with an orifice located just inside the base of the sting fairing.

TESTS

Longitudinal force and moment characteristics were measured through an angle-of-attack range from -3° to $+28^\circ$. Lateral-directional characteristics were measured through an angle-of-sideslip range from -4° to $+19^\circ$ at angles, of attack of 0°, 6°, and 12° and through an angle-of-attack range from -4° to $+18^\circ$ at an angle of sideslip of 6°. The investigation was made over a Mach number range of 0.25 to 0.90 at a Reynolds number of 3.3×10^6, and over a Reynolds number range of 0.7×10^6 to 16.0×10^6 at a Mach number of 0.25. Results were obtained for both models with vertical surfaces, small canopy, and longitudinal-control surfaces having 25 percent of the basic disk area. Component studies were made with the model having a thickness-diameter ratio of 0.225 and included tests with vertical surfaces off, large canopy, and longitudinal-control surfaces having 20 percent of the basic disk area. The tests were conducted with the models in a clean condition, that is, without devices designed to fix the location of boundary-layer transition.

CORRECTIONS TO DATA

The data have been corrected by the method of reference 8 for wind-tunnel-wall interference associated with lift on the model. The magnitudes of the corrections which were added to the measured values are as follows:

$$\Delta\alpha = 0.21\ C_L$$

$$\Delta C_D = 0.0036\ C_L^2$$

Corrections to the data to account for the effects of constriction due to the wind-tunnel walls were calculated by the method of reference 9. At a mach number of 0.90, the correction amounted to an increase of about 1.5 percent in the measured value of Mach number and dynamic pressure.

The drag data have been adjusted to correspond to a pressure at the base of the cylindrical sting fairing equal to free-stream static pressure.

The reference area used for the adjustment was the cross-sectional area of the sting fairing. In the region of maximum lift-drag ratio the base-pressure adjustment increased the drag by about 5 percent at low speeds and altered the drag by less than 2 percent at high subsonic speeds.

RESULTS AND DISCUSSION

The results of the investigation are presented graphically in figures 4 through 20. Longitudinal aerodynamic characteristics of the model with a thickness-diameter ratio of 0.225 are presented in figures 4 through 9 and those of the model with a thickness-diameter ratio of 0.325 are presented in figures 10 and 11. Lift- and pitching-moment-curve slopes and lift-drag characteristics for both models are shown as functions of Mach number in figures 12 and 13. Lateral-directional characteristics of the model with a thickness-diameter ratio of 0.225 are presented in figures 14 through 17 and those of the model with a thickness-diameter ratio of 0.325 are shown in figures 18 and 19. Figure 20 summarizes the lateral-directional stability derivatives for both models for the range of Mach numbers. Data for the basic disk shapes without appendages were taken from reference 3.

Longitudinal Characteristics

Effects of Reynolds number.- The effects of increasing Reynolds number on the longitudinal aerodynamic characteristics of the models were evidenced by increases in lift-drag ratio and small negative shifts in zero-lift pitching moment. These effects are shown in figure 4, wherein data are presented for the thinner model with 20-percent flaps at Reynolds numbers from 0.7×10^6 to 16×10^6 at a Mach number of 0.25 and at Reynolds numbers of 3.3×10^6 and 7.1×10^6 at a Mach number of 0.60. Further evidence of these effects can be seen by a comparison of the results at a Reynolds number of 3.3×10^6 with those at 16×10^6, that is, figure 8(a) with 8(b) for the thinner model having 25-percent flaps, and figure 10(a) with 10(b) for the thicker model having 25-percent flaps.

Effects of configuration changes.- The effects of vertical surfaces, canopy shape, and flap size on the aerodynamic characteristics of the model having a maximum thickness-diameter ratio of 0.225 are shown in figures 5, 6, and 7, respectively. The addition of vertical surfaces on the model resulted in more negative zero-lift pitching moments and small minimum-drag increases throughout the subsonic speed range. At low speeds, increases in lift-curve slope and in longitudinal stability at low lift coefficients, and reductions in induced drag resulted from addition of the vertical surfaces. A comparison of the results obtained

on the model incorporating a small streamlined canopy with the results obtained on the model with a larger spherical canopy (fig. 6) shows that large drag penalties were associated with the larger canopy, particularly at high subsonic speeds. In addition, the model with the larger canopy had higher angles of attack for zero lift and generally more negative pitching moments at zero lift. Increasing the longitudinal-control (flap) surface area from 20 to 25 percent of the basic disk area resulted in significantly improved characteristics as shown in figure 7. Use of the larger flaps resulted in increases in lift-curve slope, large improvements in longitudinal stability, and higher lift-drag ratios at lift coefficients above those for maximum lift-drag ratio at high subsonic speeds.

Effects of Mach number.- The data for several control deflections presented in figures 8 and 9 for the thinner model and in figures 10 and 11 for the thicker model show that, with the moment center located at 40 percent of the diameter, both models were statically stable at low subsonic speeds. In general, the stability at low speeds increased with increasing lift coefficient. Increasing the Mach number to 0.60 resulted in some reduction in stability, notably at high lift coefficients. In the range of Mach numbers from 0.80 to 0.90, both models exhibited varying degrees of instability up to the region near maximum lift, wherein a stable trend in the pitching moments normally occurred. Upward deflection of the flaps from 0° to -10° resulted in large increases in trim lift coefficient at low speeds, but in some cases resulted in decreases in trim lift coefficient at high subsonic speeds. At all Mach numbers, flap deflection had little effect on the slope of the pitching-moment curve, but generally resulted in increases in zero-lift angle of attack. When compared with the basic disks, both model configurations showed large improvements in lift and stability characteristics as shown in figures 8 to 12. In figure 12 the slopes of the lift curves represent average values between angles of attack of 0° and 5° and the slopes of the pitching-moment curves represent average values between lift coefficients of 0 and 0.1. In this region of low lift coefficients the lift-curve slopes for the model configurations were in some instances over twice as high as those for the basic disks, and whereas the basic disks exhibited a large degree of instability, the model configurations as previously noted, were slightly stable at low speeds and slightly unstable at high subsonic speeds.

It may be further noted in figures 8 to 11 that at low speeds, deflection of the flap resulted in only small reductions in lift-drag ratio. In the Mach number range from 0.60 to 0.90, the losses associated with flap deflection increased progressively. At low speeds and for a lift coefficient of about 0.4, the trim lift-drag ratio for the model configuration having a thickness-diameter ratio of 0.225 was 6 (fig. 8(b)), and that for the thicker model was almost 5 (fig. 10(b)). Further examination of figures 8 to 11 and 13, which summarizes the lift-drag characteristics in terms of Mach number, reveals that when compared with

the basic disks, both model configurations had lower values of maximum lift-drag ratio throughout most of the Mach number range. However, because the induced drag of the model configurations was lower than that of the basic disks, improvements in lift-drag ratio were evidenced at lift coefficients above those for maximum lift-drag ratio.

Lateral Characteristics

It may be seen in figure 14 that the lateral-directional characteristics, that is, the yawing-moment, rolling-moment, and side-force coefficients were somewhat insensitive to changes in Reynolds number from 3.3×10^6 to 16×10^6. While these data are for the thinner model with 20-percent flaps, whereas the following discussion on lateral-directional characteristics pertains to the models with 25-percent flaps, it is shown in figure 15 that the differences between the lateral-directional characteristics associated with the 20- and 25-percent flaps were generally small throughout the angle-of-sideslip range investigated.

The lateral-directional characteristics are presented as functions of angle of attack for a constant sideslip angle of 6° in figure 16 for the thinner model and in figure 18 for the thicker model. The data show that the yawing-moment and side-force coefficients were insensitive to angle of attack and the rolling-moment coefficients increased essentially linearly with increasing angle of attack. Comparison of the results obtained for the model incorporating vertical surfaces with those obtained for the model with no vertical surfaces (fig. 16) shows, as anticipated, that the vertical surfaces were primarily responsible for the directional stability of the model. The lateral-directional characteristics are shown as functions of sideslip angle for several angles of attack in figure 17 for the thinner model, and in figure 19 for the thicker model. At low speeds the coefficients increased essentially linearly with sideslip angle; in the Mach number range from 0.60 to 0.80 the coefficients increased smoothly up to a sideslip angle of about 15°, above which reductions frequently occurred, particularly for the thicker model. A summary of the lateral data is shown in figure 20 as lateral-directional stability derivatives at an angle of attack of 6° as functions of Mach number. It is evident that both models had directional stability and positive effective dihedral throughout the Mach number range at this angle of attack.

CONCLUSIONS

Results of an investigation of two disk-shaped re-entry configurations employing trailing-edge control surfaces, vertical surfaces, and canopies at angles of attack to 28° and angles of sideslip to 19° can be summarized as follows:

1. With the moment center at 40 percent of the diameter, both models were longitudinally stable at low subsonic speeds. In the range of Mach numbers from 0.80 to 0.90, the models exhibited varying degrees of instability up to the region near maximum lift, wherein a stable trend in the pitching moments normally occurred. In contrast to the stability characteristics of both model configurations, the basic disk shapes were very unstable throughout the entire subsonic speed range.

2. At low speeds, deflection of the trailing-edge flap resulted in only small reductions in lift-drag ratio and provided an effective means for trim change.

3. At low speeds and for a lift coefficient of about 0.4, the trim lift-drag ratio for the model having a thickness-diameter ratio of 0.225 was 6, and that for the model having a thickness-diameter ratio of 0.325 was almost 5.

4. Increasing the Reynolds number from 0.7×10^{6} to 16×10^{6} resulted in substantial increases in lift-drag ratio and small negative shifts in zero-lift pitching moment at low speeds.

5. Both models had directional stability and positive effective dihedral throughout the Mach number range.

Ames Research Center
National Aeronautics and Space Administration
Moffett Field, Calif., April 7, 1961

REFERENCES

1. Chapman, Dean R.: An Analysis of the Corridor and Guidance Requirements for Supercircular Entry Into Planetary Atmospheres. NASA TR R-55, 1960.

2. Chapman, Dean R.: An Approximate Analytical Method for Studying Entry Into Planetary Atmospheres. NASA TR R-11, 1959. (Supersedes NACA TN 4276)

3. Demele Fred A., and Brownson, Jack J.: Subsonic Longitudinal Aerodynamic Characteristics of Disks With Elliptic Cross Sections and Thickness-Diameter Ratios From 0.225 to 0.425. NASA TN D-788, 1961.

4. Ware, George M.: Static Stability and Control Characteristics at Low-Subsonic Speeds of a Lenticular Reentry Configuration. NASA TM X-431, 1960.

5. Mugler, John P., Jr., and Olstad, Walter B.: Static Longitudinal Aerodynamic Characteristics at Transonic Speeds of a Lenticular-Shaped Reentry Vehicle. NASA TM X-423, 1960.

6. Jackson, Charlie M., Jr., and Harris, Roy V., Jr.: Static Longitudinal Stability and Control Characteristics at a Mach Number of 1.99 of a Lenticular-Shaped Reentry Vehicle. NASA TN D-514, 1960.

7. Lazzeroni, Frank A.: Aerodynamic Characteristics of Two Disk Re-entry Configurations at a Mach Number of 2.2. NASA TM X-567, 1961.

8. Glauert, H.: The Elements of Aerofoil and Airscrew Theory. Macmillan Company, N.Y., 1943, p. 191.

9. Herriot, John G.: Blockage Corrections for Three-Dimensional-Flow Closed Throat Wind Tunnels, With Consideration of the Effect of Compressibility. NACA Rep. 995, 1950. (Supersedes NACA RM A7B28).

TABLE I.- COORDINATES OF SURFACE OF MODELS
[All dimensions in inches]

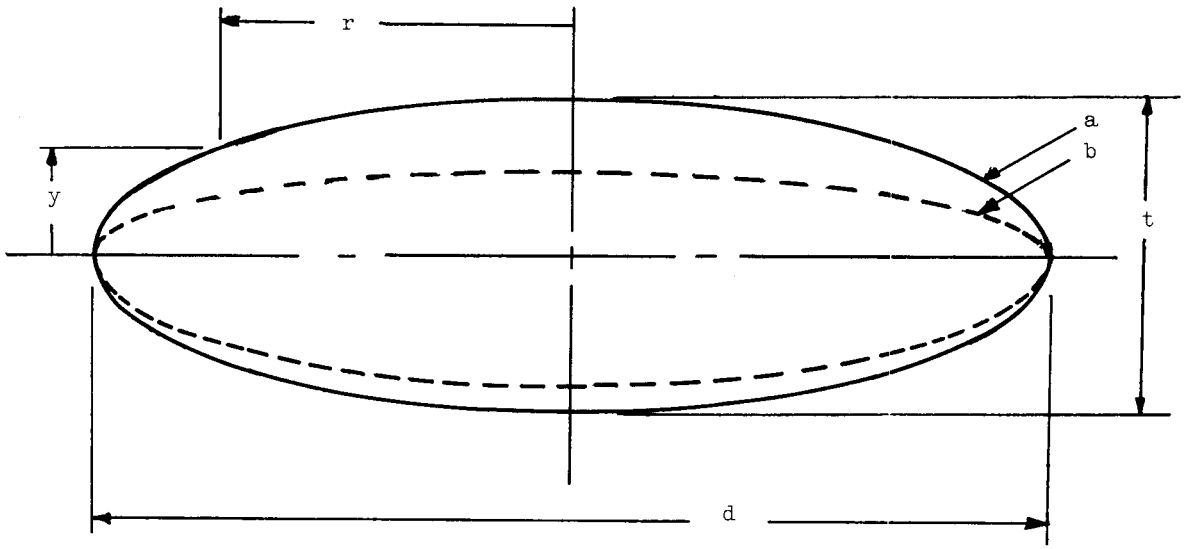

r	t/d = 0.325	t/d = 0.225		r	t/d = 0.325	t/d = 0.225	
	$\pm y_a$	y_b	$-y_b$		$\pm y_a$	y_b	$-y_b$
0	3.90	2.10	3.30	10.00	2.16	1.16	1.82
1.00	3.89	2.09	3.29	10.50	1.89	1.02	1.60
2.00	3.84	2.07	3.25	10.75	1.73	.93	1.47
3.00	3.78	2.03	3.20	11.00	1.56	.84	1.32
4.00	3.68	1.98	3.11	11.25	1.36	.73	1.15
5.00	3.54	1.91	3.00	11.50	1.11	.60	.94
6.00	3.38	1.82	2.86	11.60	1.00	.54	.84
7.00	3.17	1.71	2.68	11.70	.87	.47	.73
7.50	3.04	1.64	2.58	11.80	.71	.38	.60
8.00	2.91	1.56	2.46	11.90	.50	.27	.42
8.50	2.75	1.48	2.33	11.95	.36	.19	.30
9.00	2.58	1.39	2.18	12.00	0	0	0
9.50	2.38	1.28	2.02				

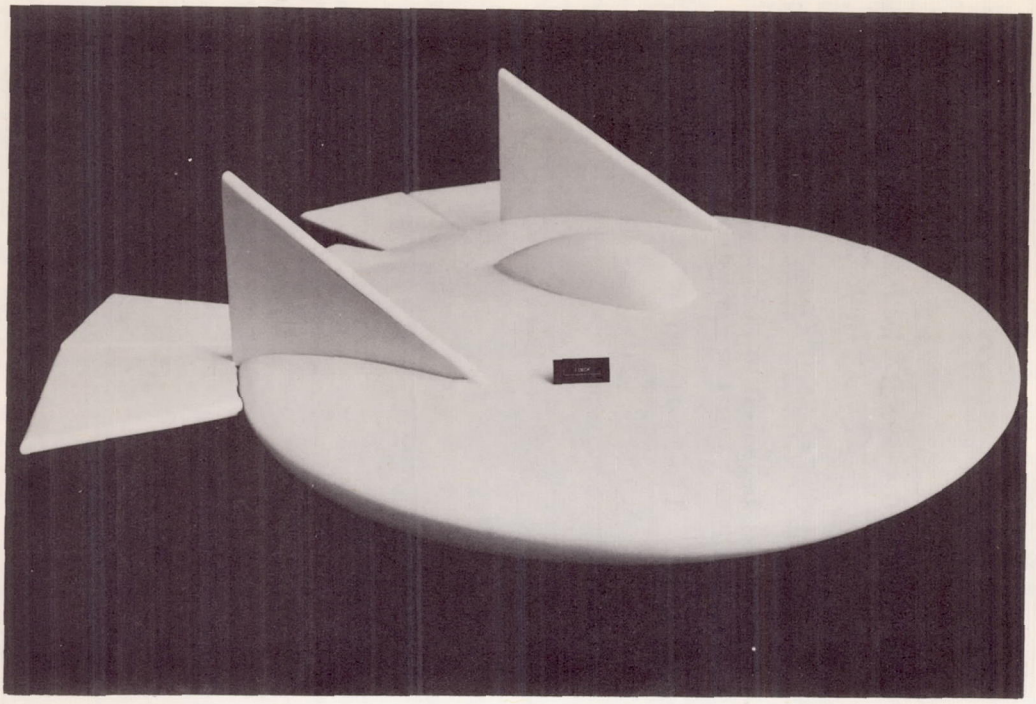

(a) t/d = 0.225 A-27284

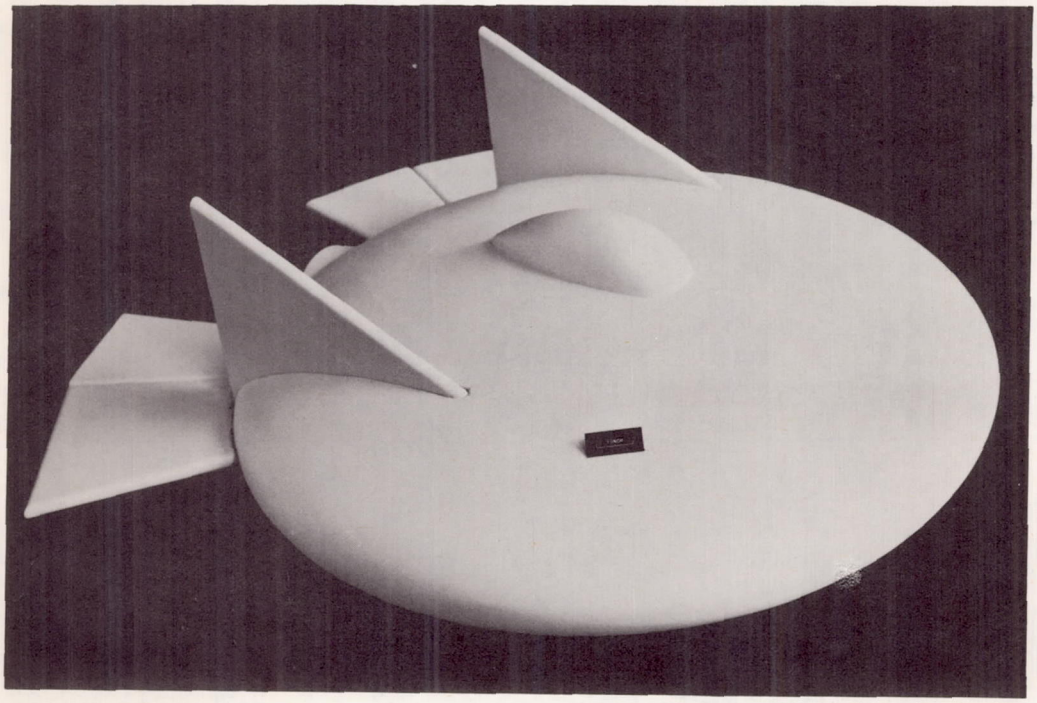

(b) t/d = 0.325 A-27282

Figure 1.- Photographs of models.

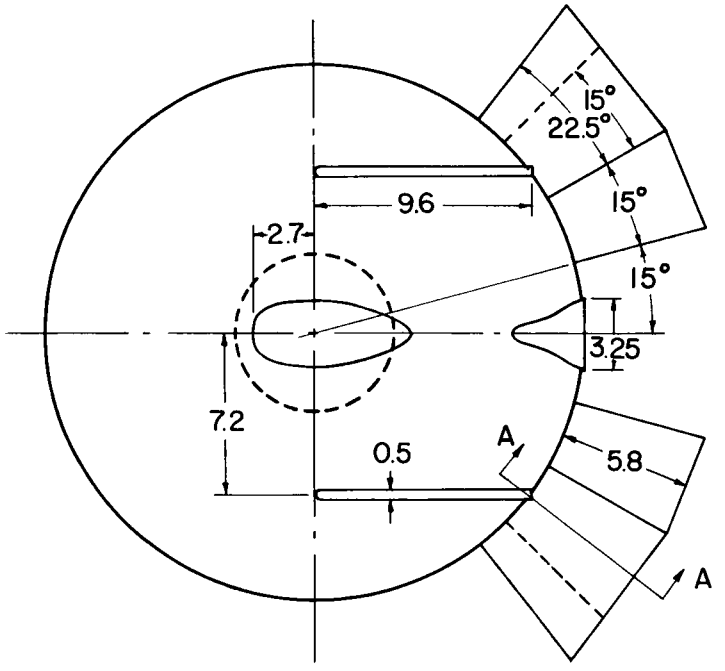

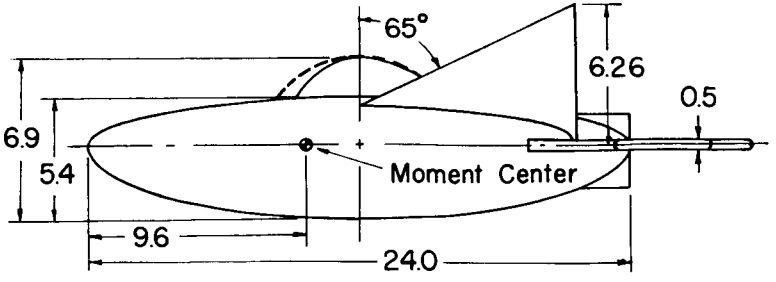

$S = 3.93$ ft^2 (with 25% Flaps)
$= 3.77$ ft^2 (with 20% Flaps)

$S_{Vert.} = 0.35$ ft^2 (Total)

$S_{Flap} = 0.79$ ft^2 (Total 25% Flaps)
$= 0.63$ ft^2 (Total 20% Flaps)

Linear dimensions in inches.

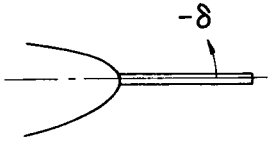

Section AA
Flap Deflection

(a) Configuration details.

Figure 2.- Geometric characteristics of the model having a thickness-diameter ratio of 0.225.

CONFIDENTIAL

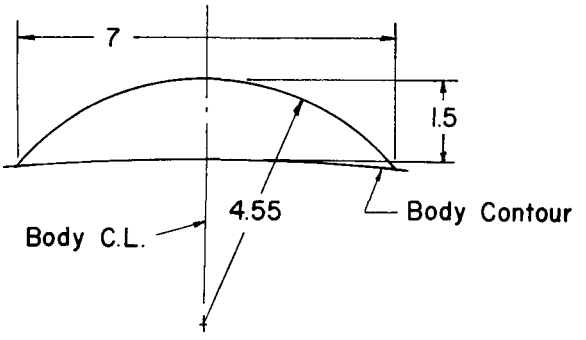

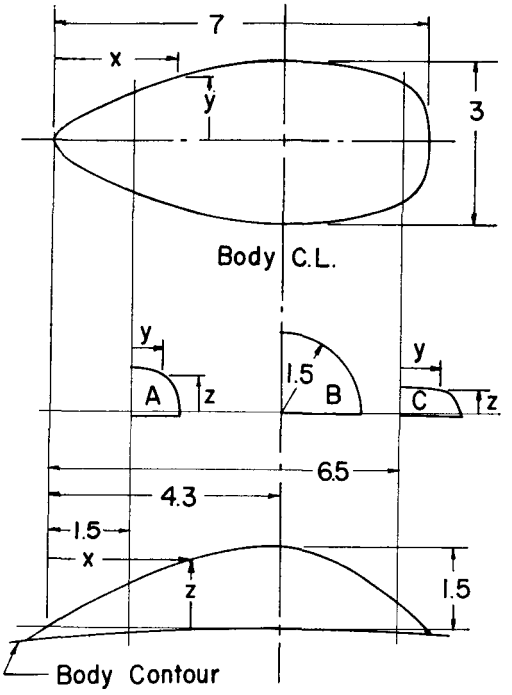

Plan		Profile		Sect. A		Sect. C	
x	y	x	z	y	z	y	z
0	0	0	0	0	0.81	0	0.49
0.1	±0.29	1.0	0.58	0.2	.80	0.2	.49
0.5	0.44	2.0	1.04	.3	.79	.4	.48
1.0	0.69	3.0	1.36	.4	.76	.5	.47
2.0	1.09	4.3	1.50	.5	.73	.6	.46
3.0	1.38	5.0	1.36	.6	.68	.7	.44
4.3	1.50	6.0	0.85	.7	.59	.8	.41
5.0	1.47	7.0	0	.8	.47	.9	.36
6.0	1.31			.9	0	1.0	.26
6.5	1.10					1.1	0
6.8	0.82						
7.0	0						

Small Canopy

(b) Canopy details.

Figure 2.- Concluded.

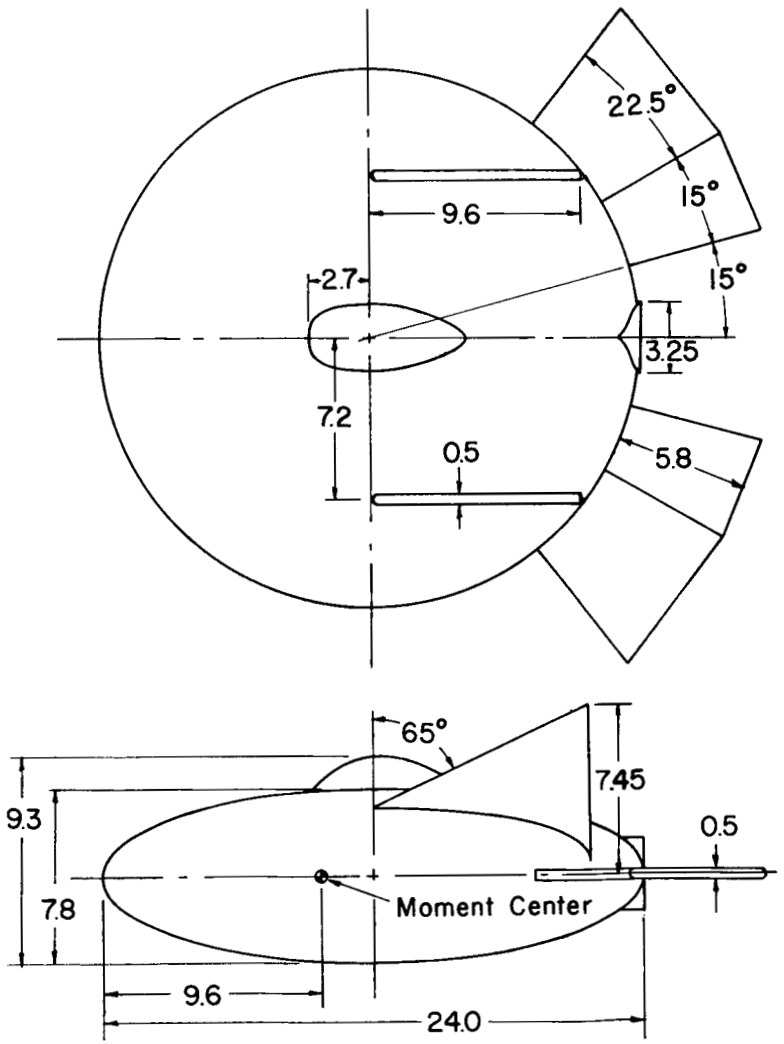

$S = 3.93\ ft^2$ (with 25% Flaps)

$S_{Vert} = 0.36\ ft^2$ (Total)

$S_{Flap} = 0.79\ ft^2$ (Total 25% Flaps)

Linear dimensions in inches.

Figure 3.- Geometric characteristics of the model having a thickness-diameter ratio of 0.325.

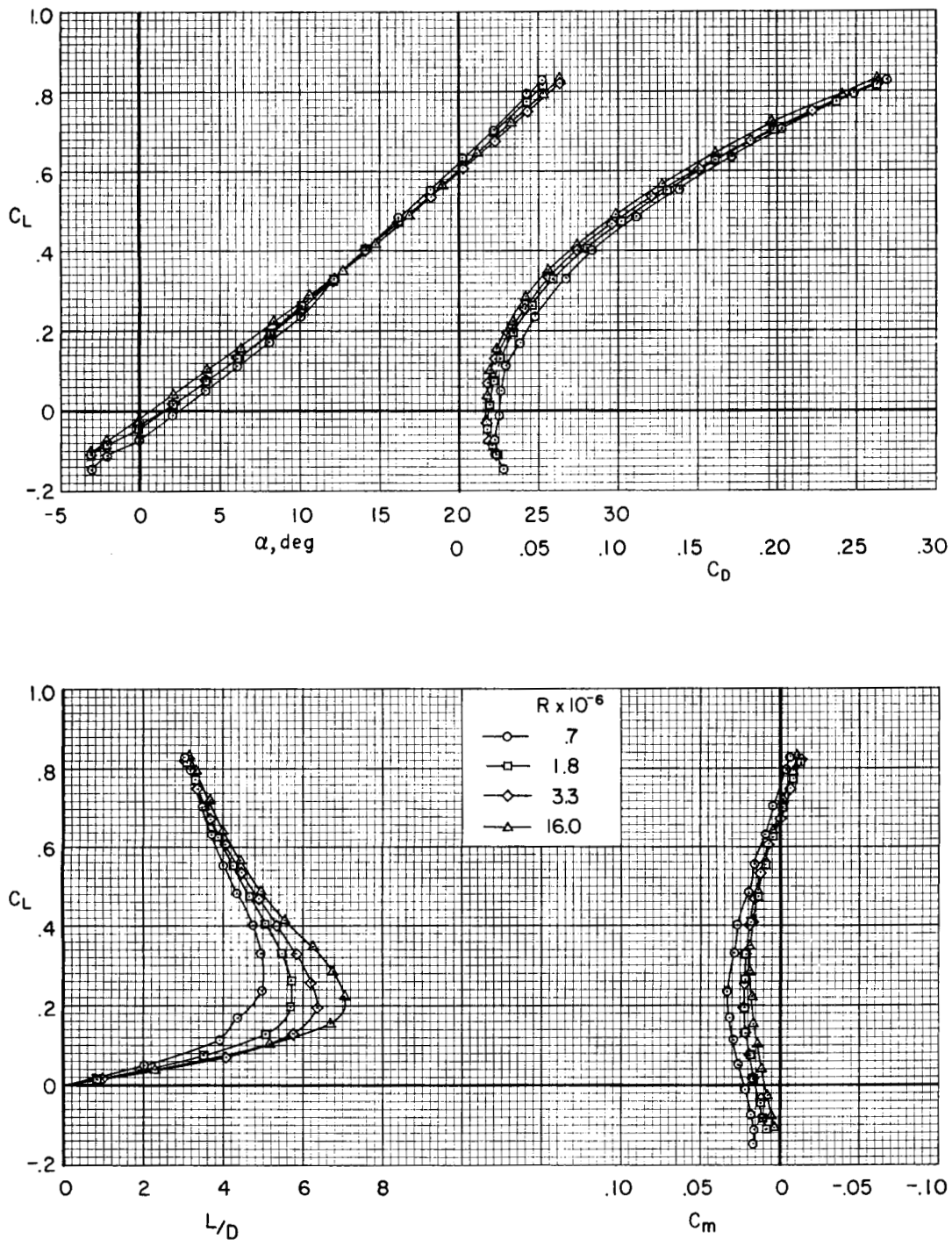

(a) M = 0.25, small canopy.

Figure 4.- The effect of Reynolds number on the longitudinal aerodynamic characteristics of the model having a thickness-diameter ratio of 0.225; 20-percent flaps; $\delta = 0^{\circ}$; vertical surfaces on.

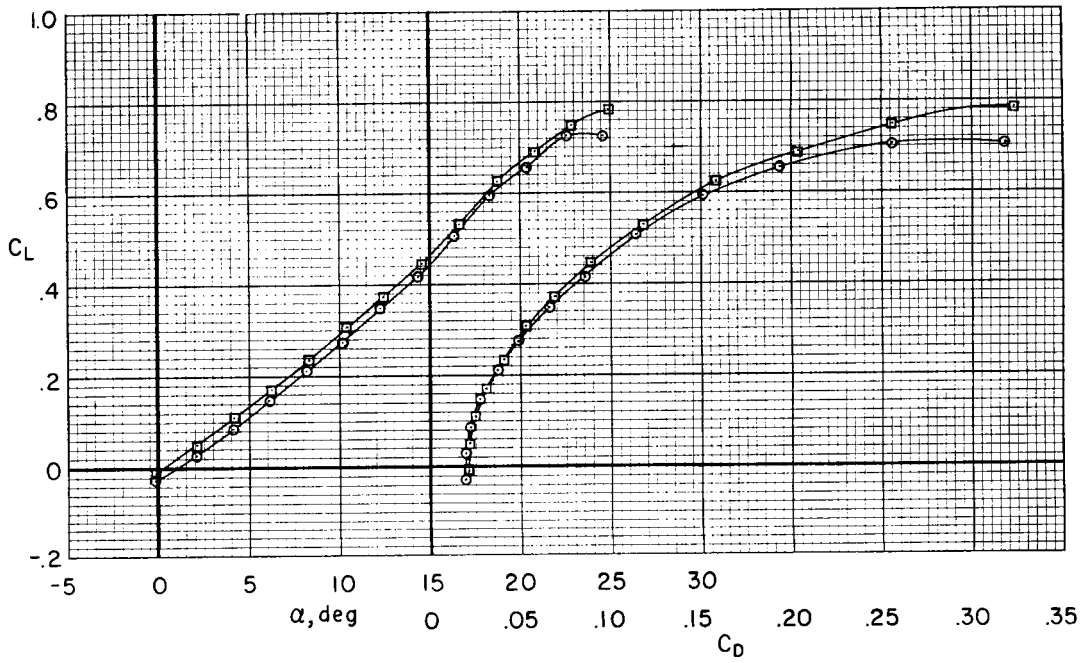

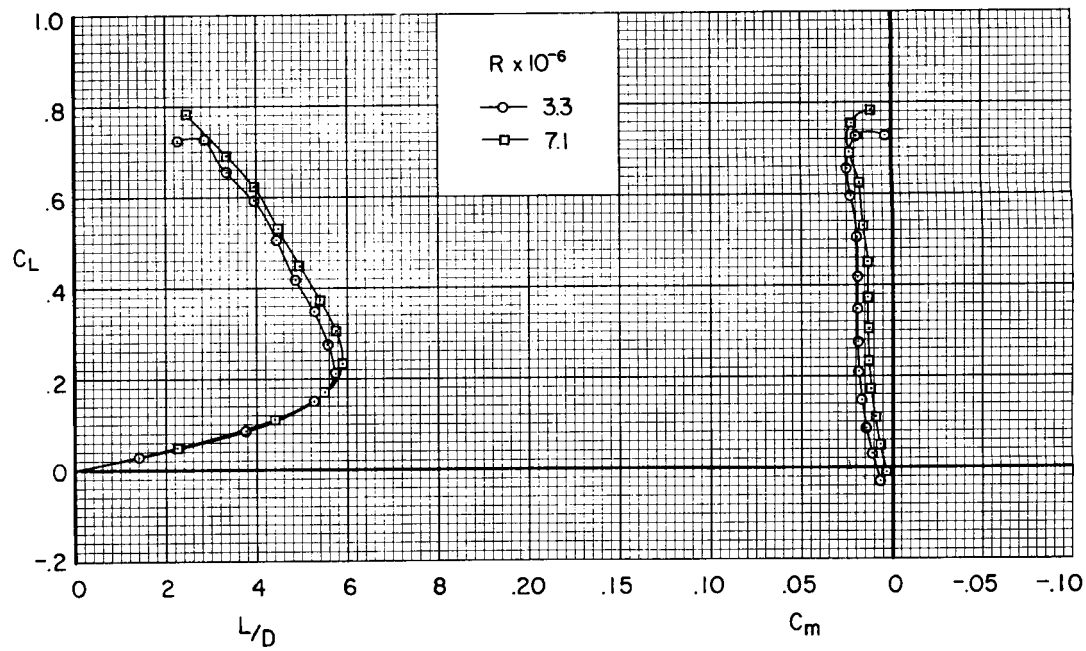

(b) M = 0.60, large canopy.

Figure 4.- Concluded.

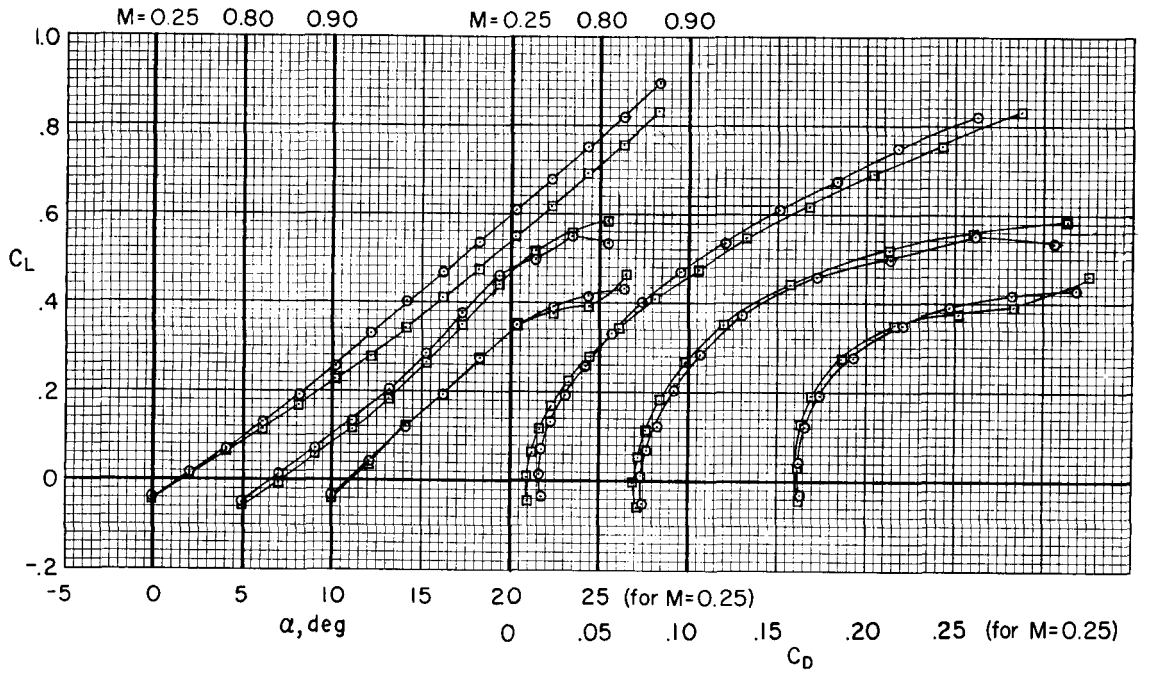

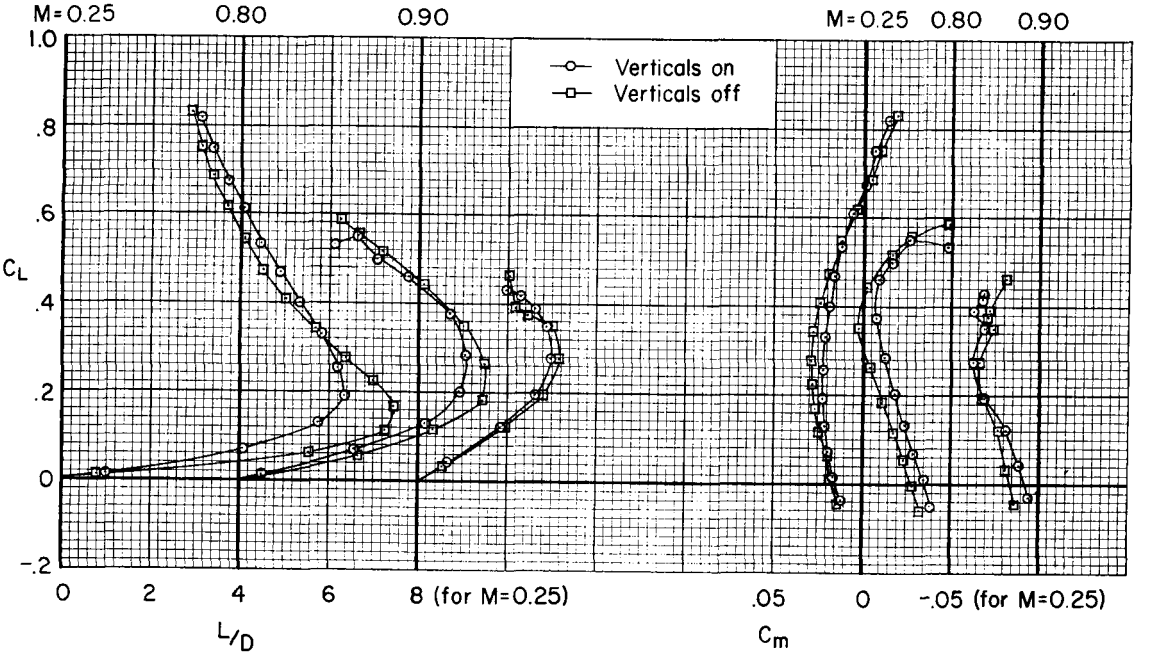

Figure 5.- The effect of vertical surfaces on the longitudinal aerodynamic characteristics of the model having a thickness-diameter ratio of 0.225; 20-percent flaps; $\delta = 0^{\circ}$; small canopy; $R = 3.3 \times 10^{6}$.

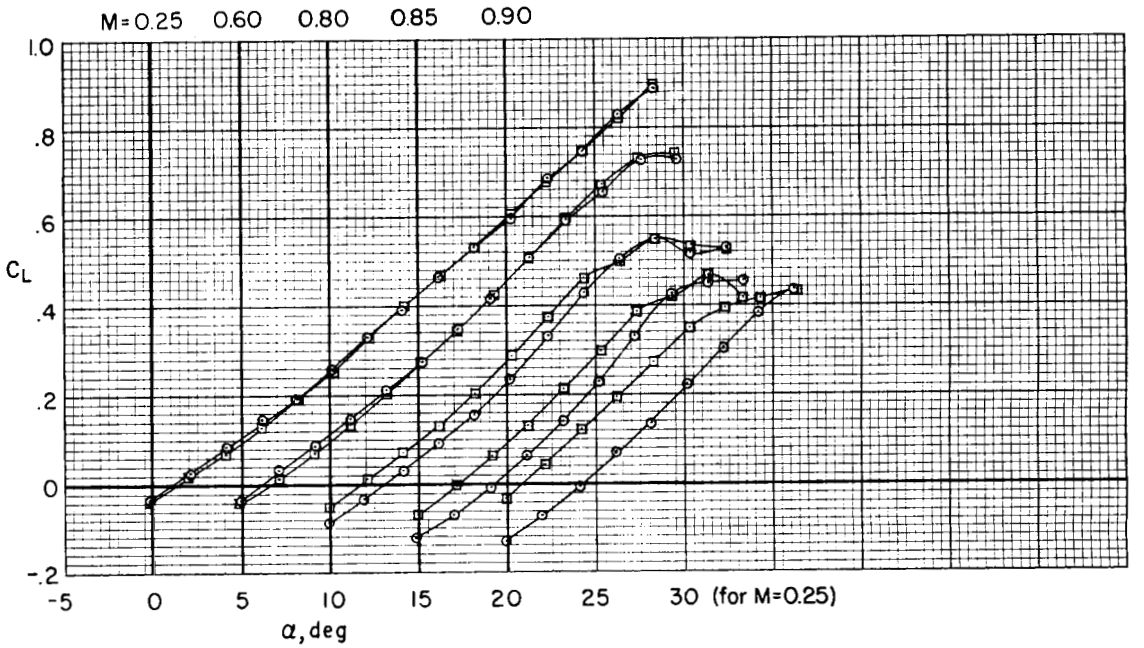

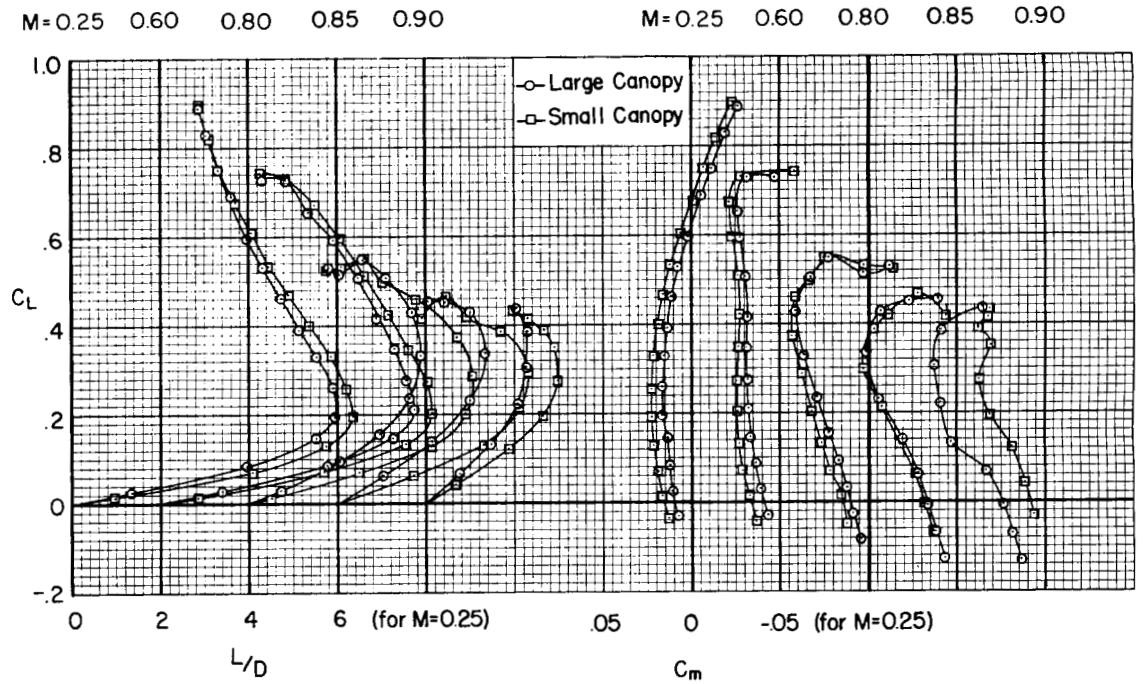

(a) C_m, L/D, α

Figure 6.- The effect of canopy shape on the longitudinal aerodynamic characteristics of the model having a thickness-diameter ratio of 0.225; 20-percent flaps; $\delta = 0^\circ$; vertical surfaces on; $R = 3.3 \times 10^6$.

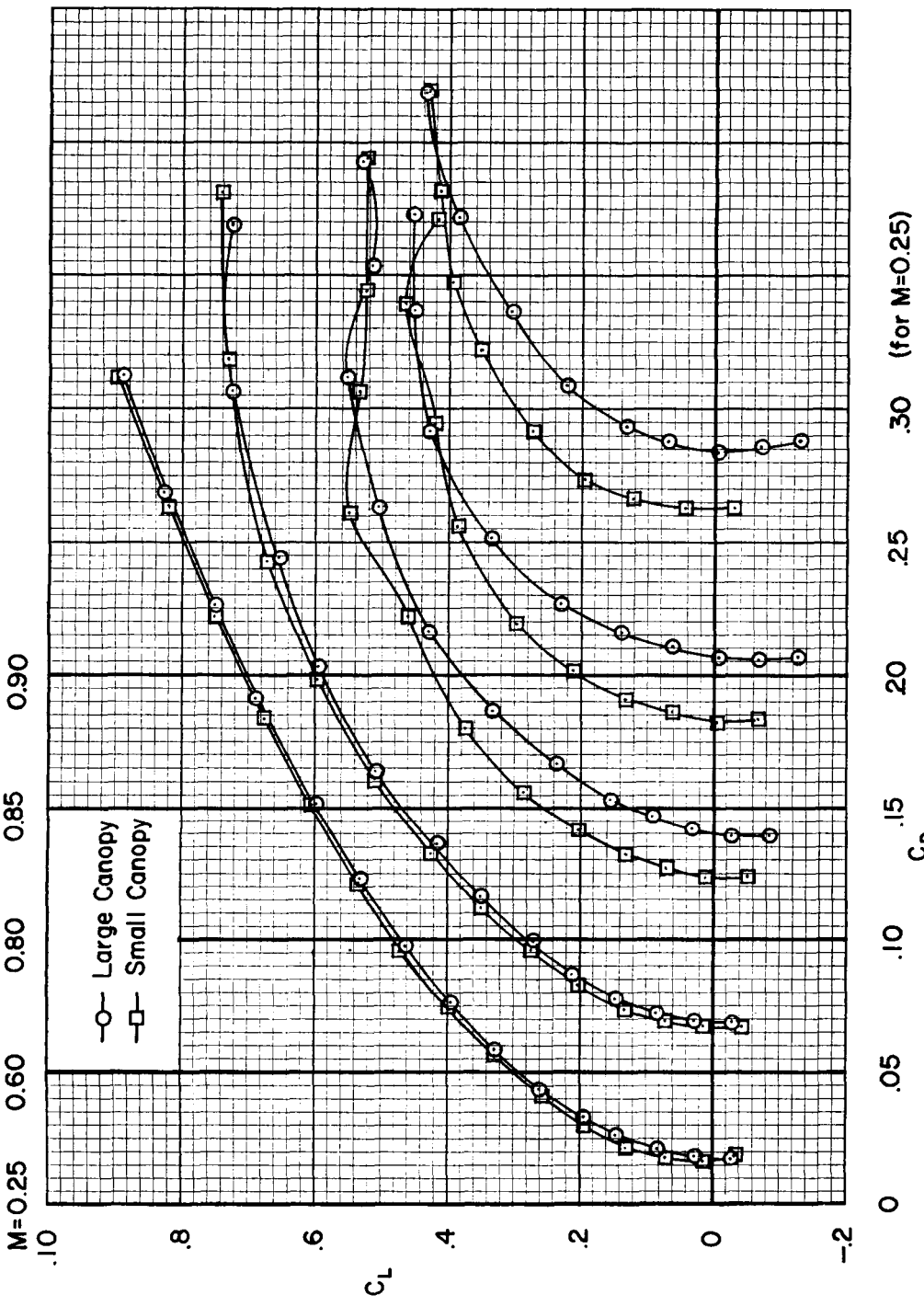

(b) C_D

Figure 6.- Concluded.

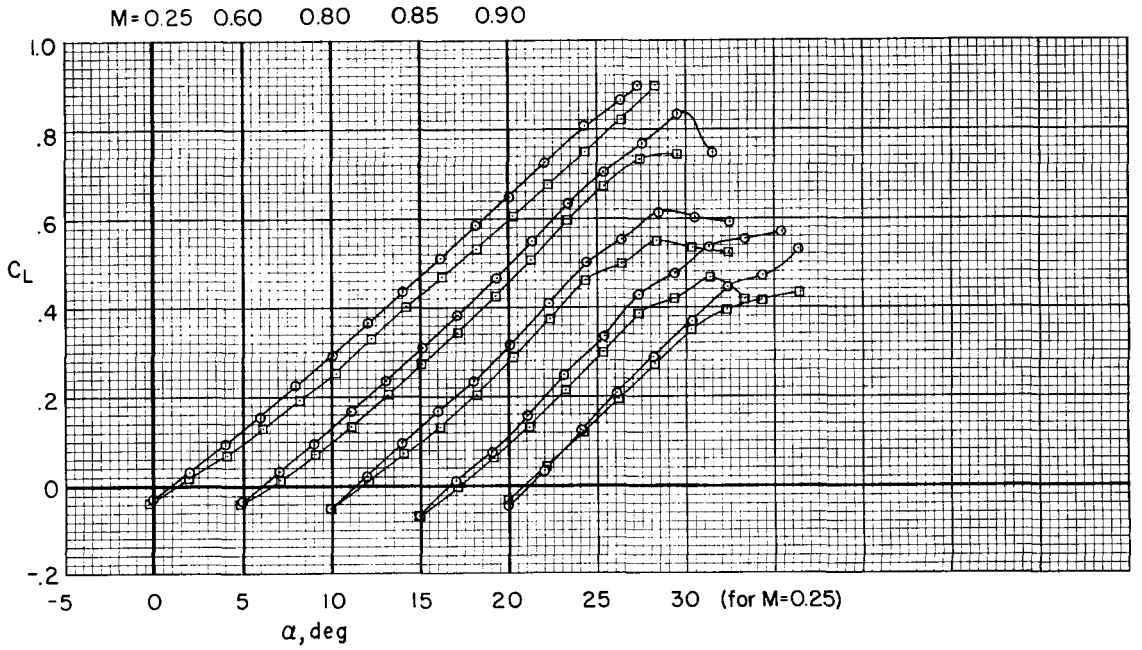

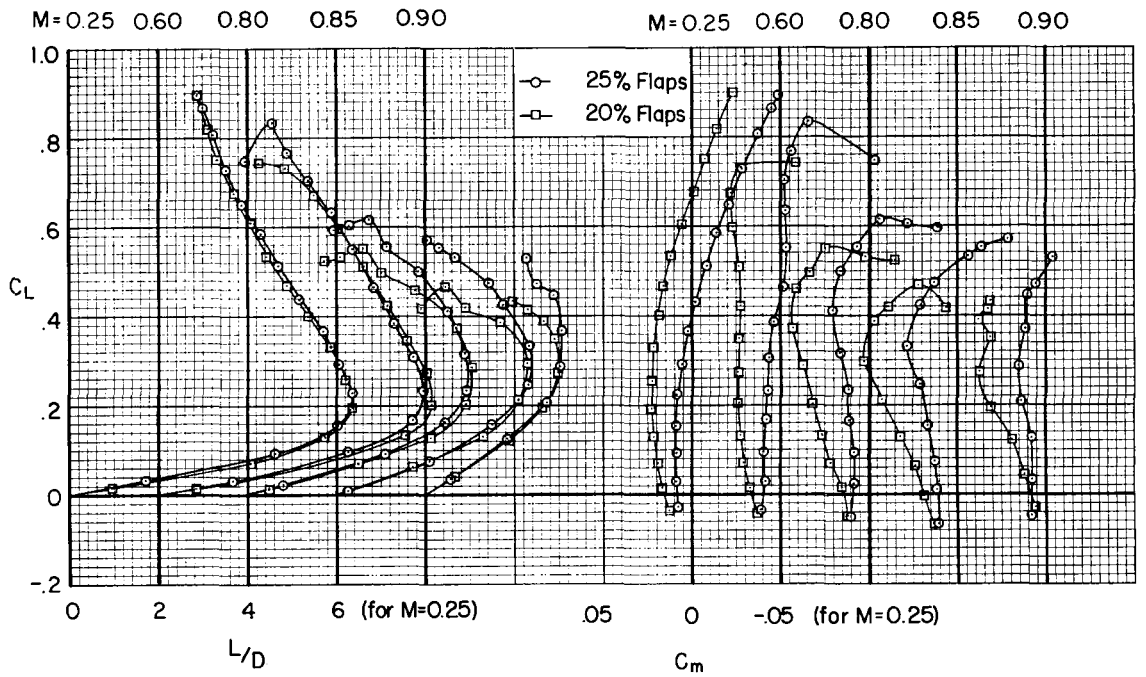

Figure 7.- The effect of flap size on the longitudinal aerodynamic characteristics of the model having a thickness-diameter ratio of 0.225; $\delta = 0^{o}$; small canopy; vertical surfaces on; $R = 3.3 \times 10^{6}$.

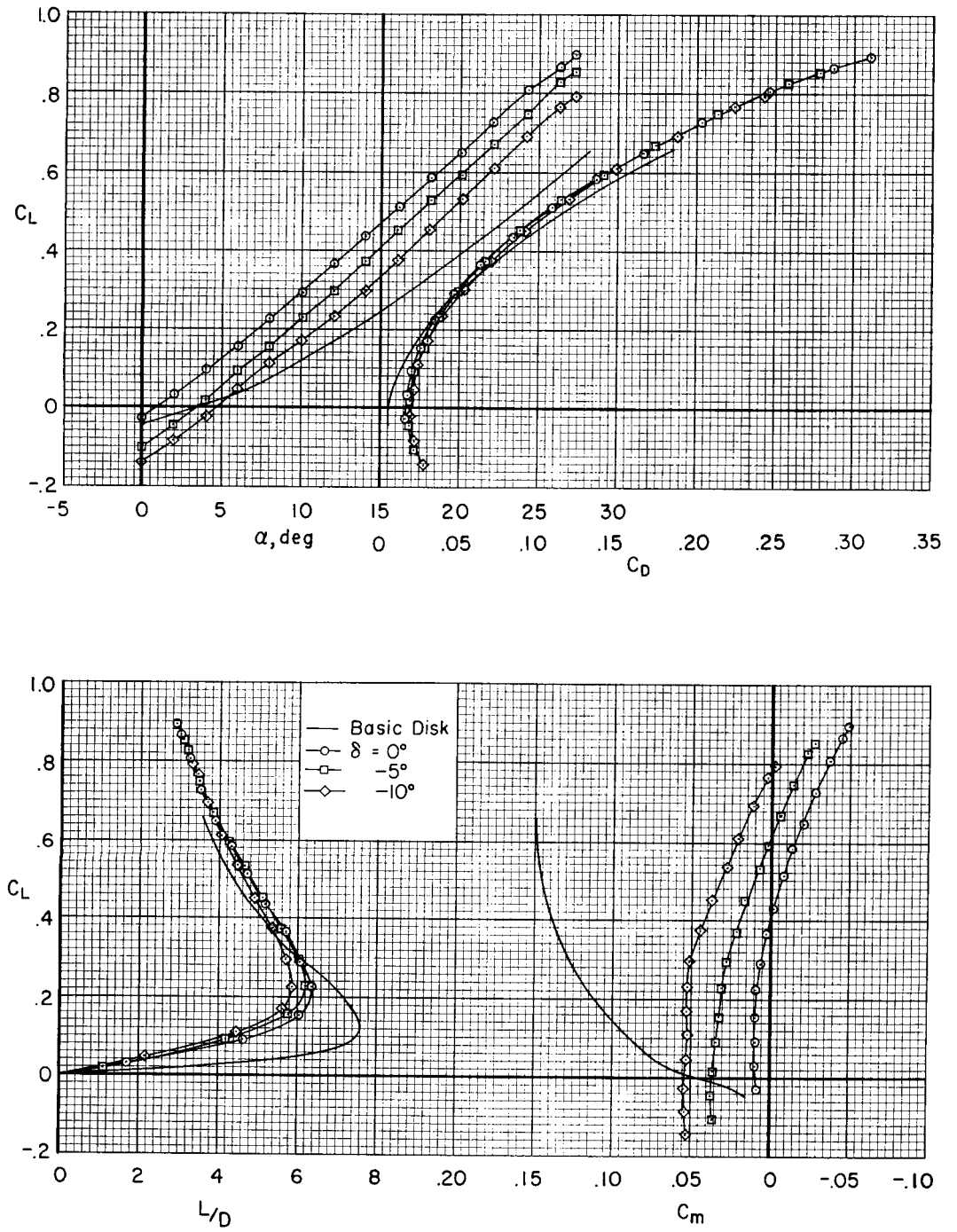

(a) $R = 3.3 \times 10^6$

Figure 8.- The longitudinal aerodynamic characteristics of the model and basic disk having a thickness-diameter ratio of 0.225; 25-percent flaps; small canopy; vertical surfaces on; M = 0.25.

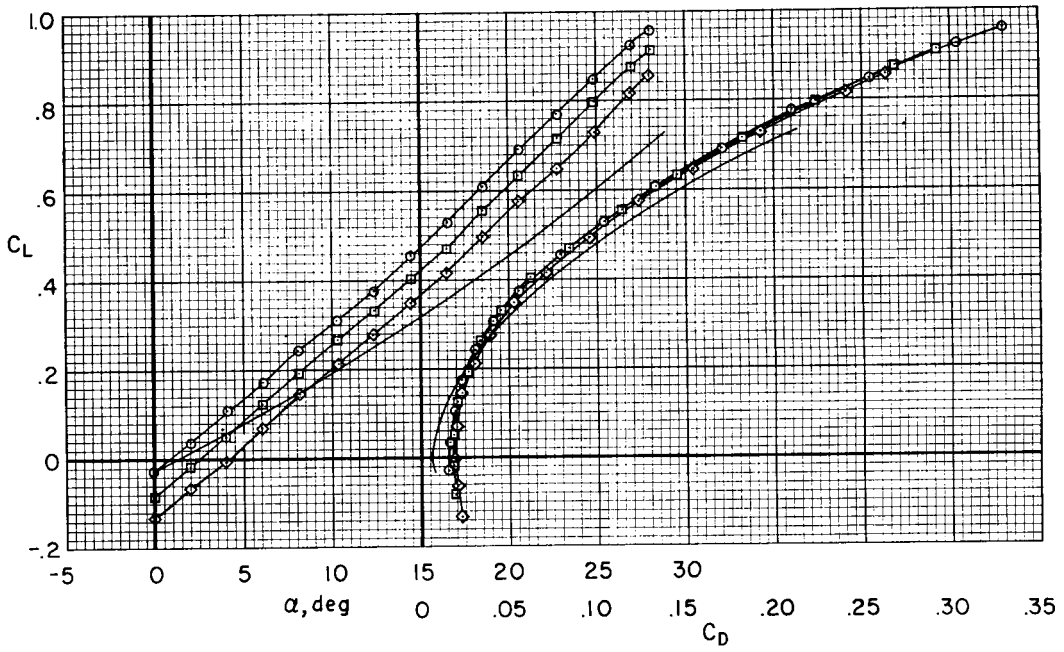

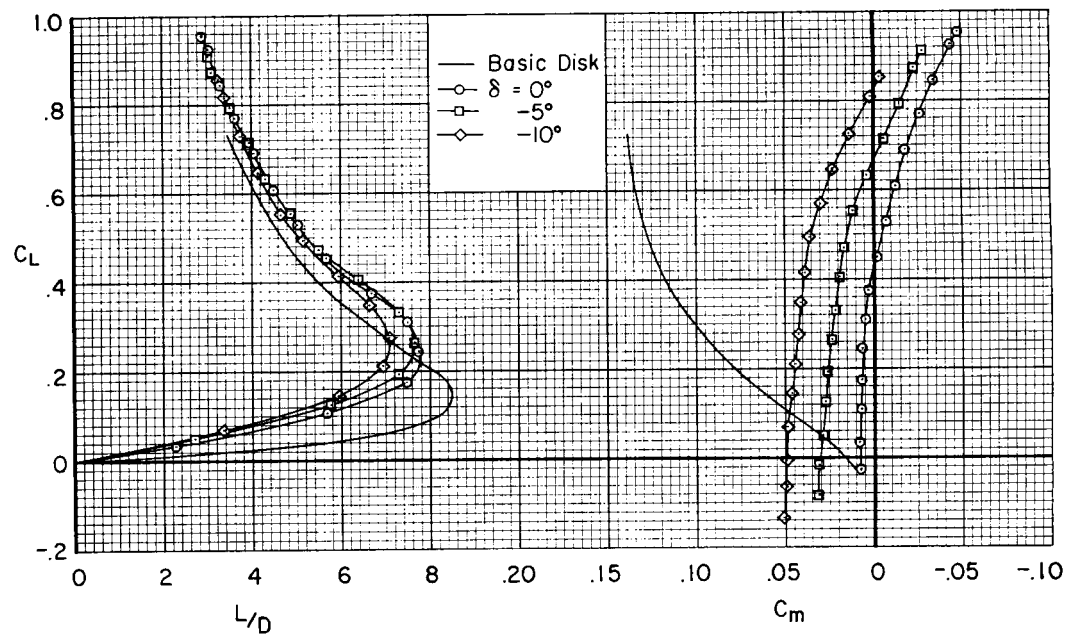

(b) R = 16×10^6

Figure 8.- Concluded.

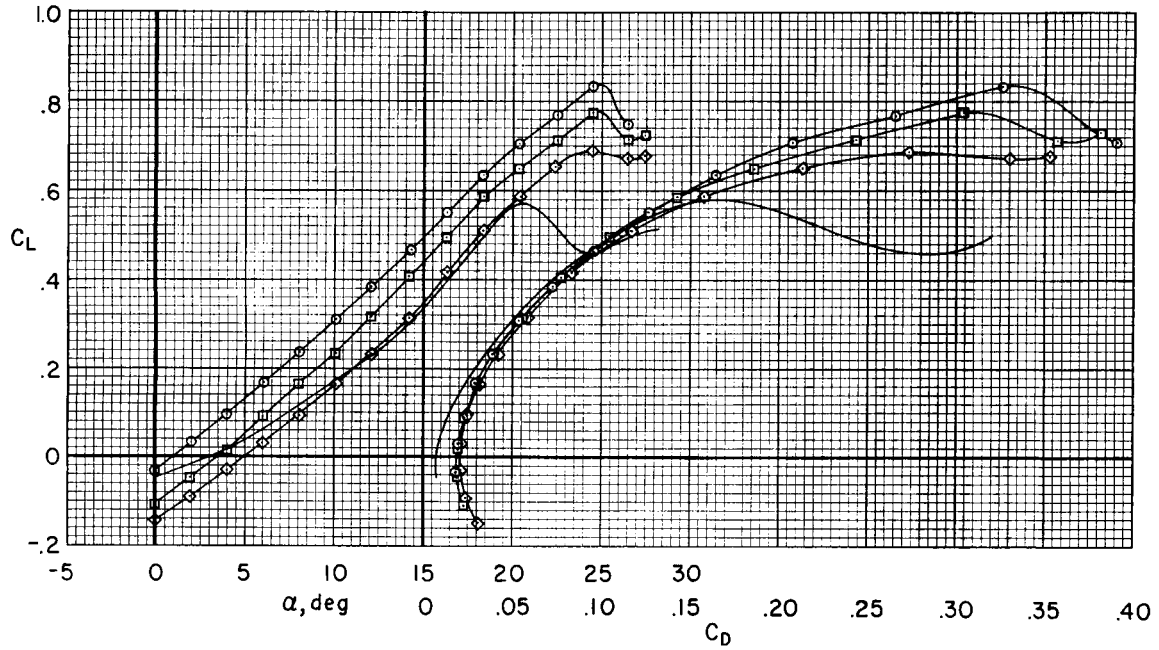

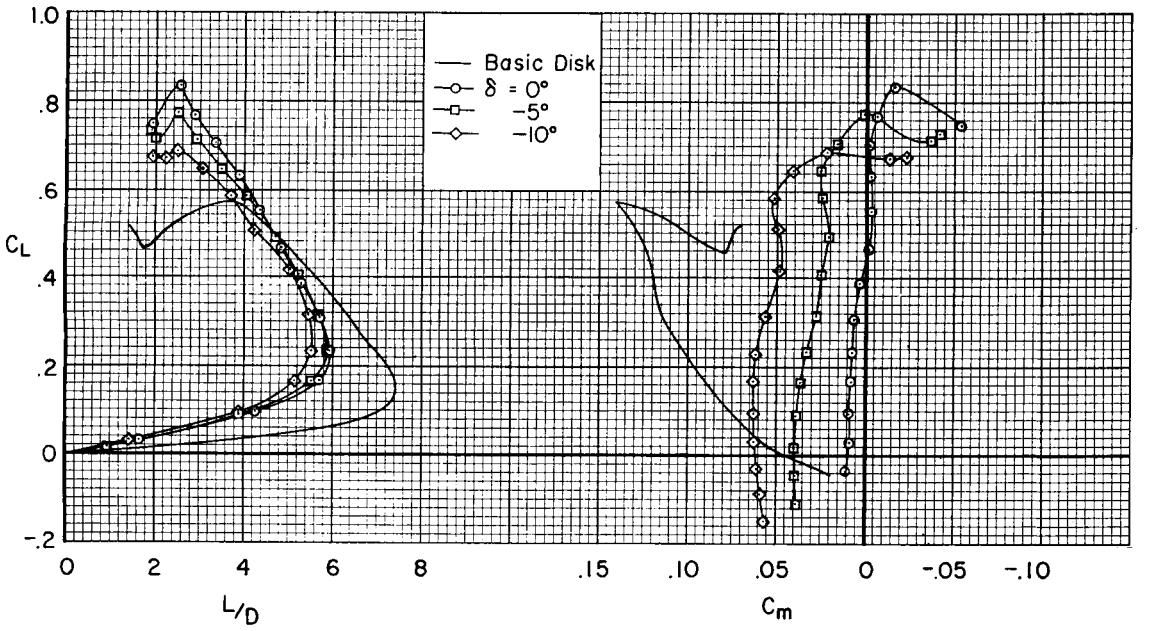

(a) $M = 0.60$

Figure 9.- The longitudinal aerodynamic characteristics of the model and basic disk having a thickness-diameter ratio of 0.225; 25-percent flaps; small canopy; vertical surfaces on; $R = 3.3 \times 10^6$.

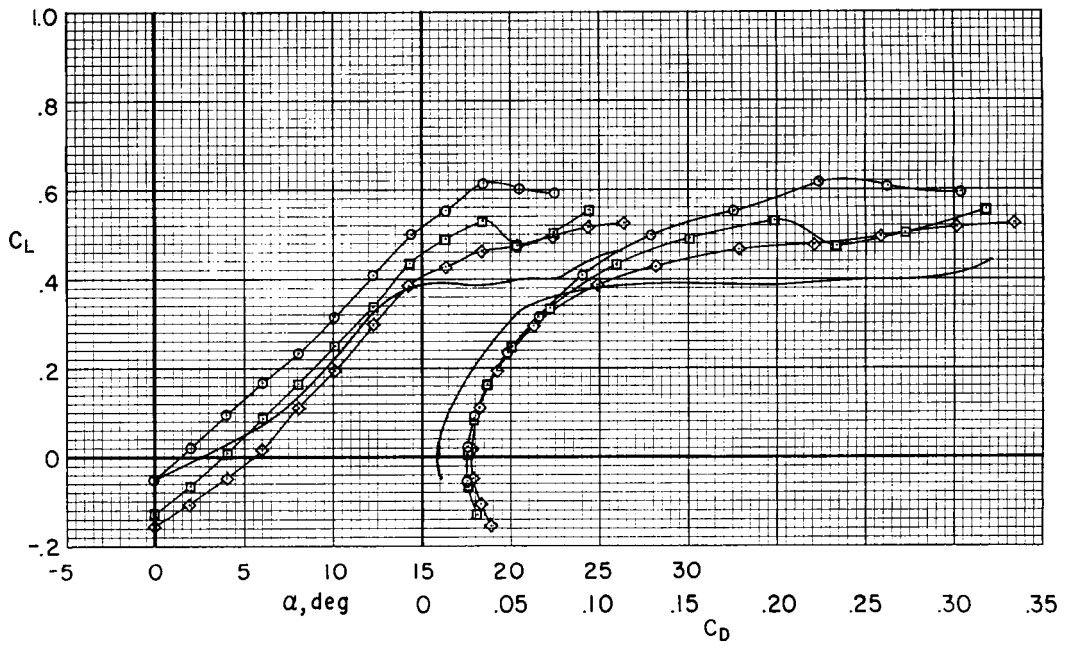

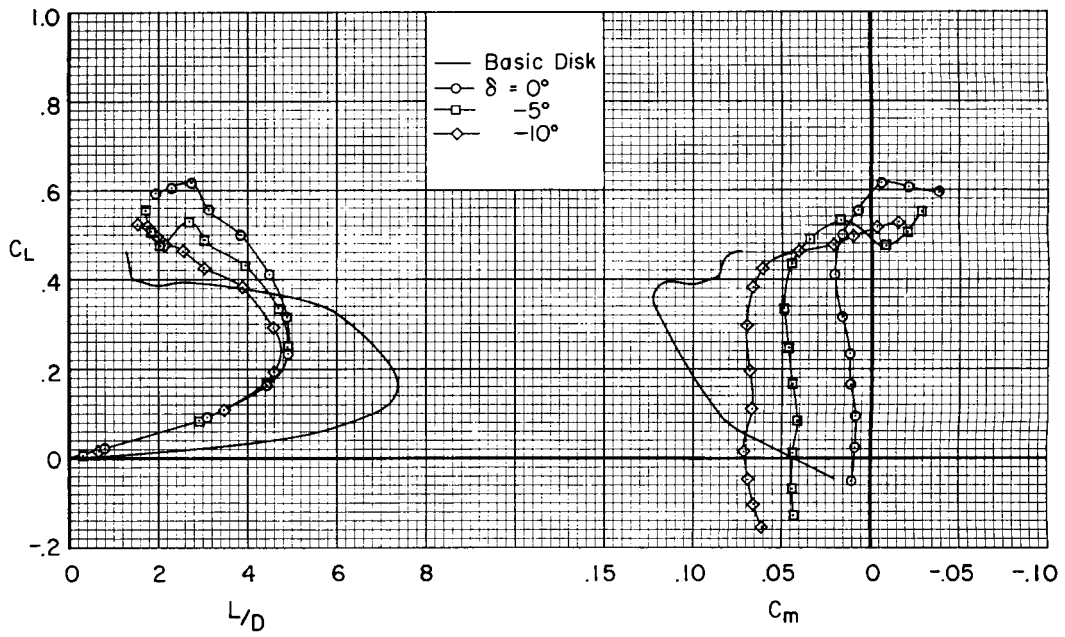

(b) M = 0.80

Figure 9.- Continued.

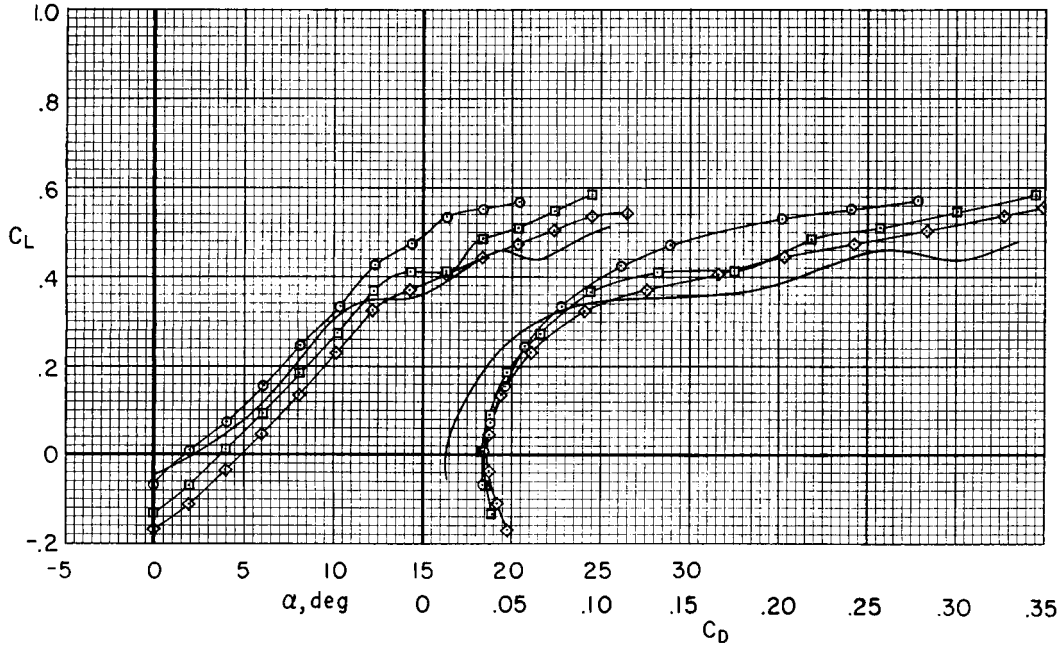

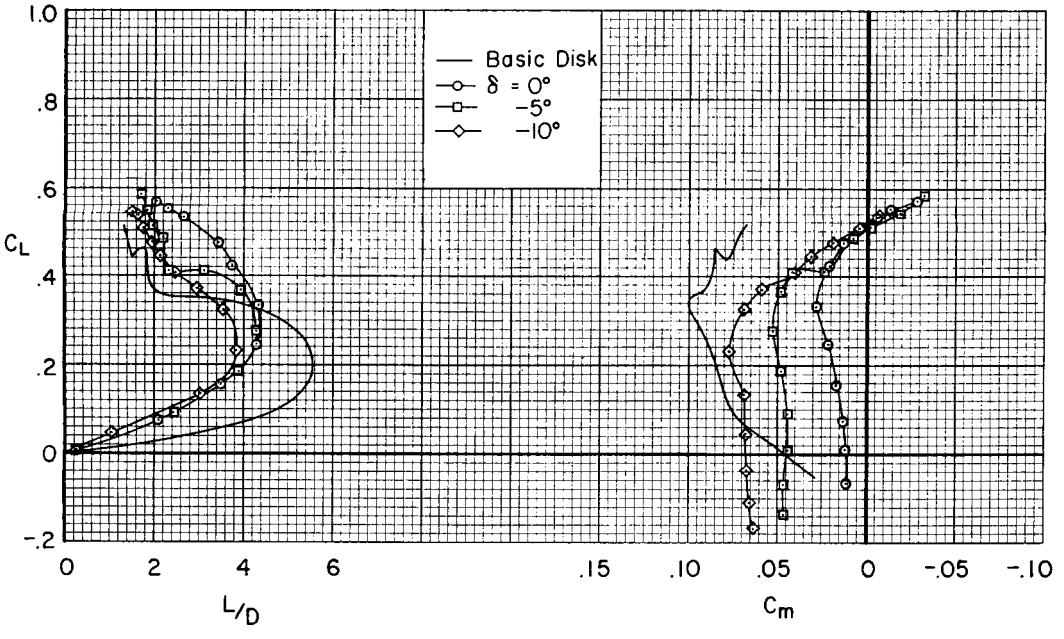

(c) M = 0.85

Figure 9.- Continued.

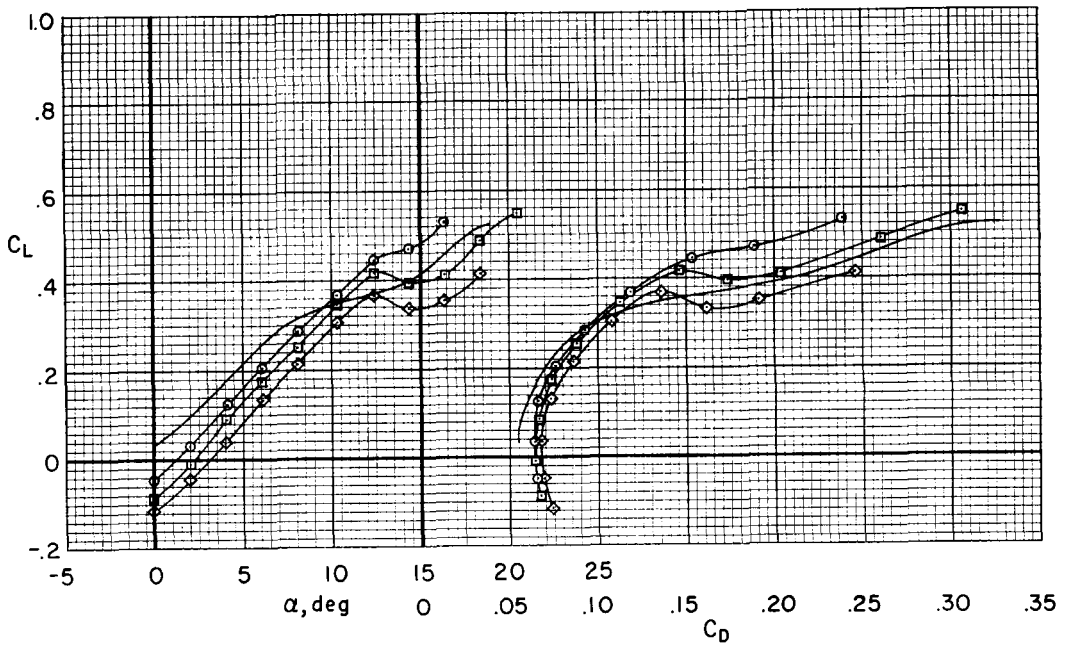

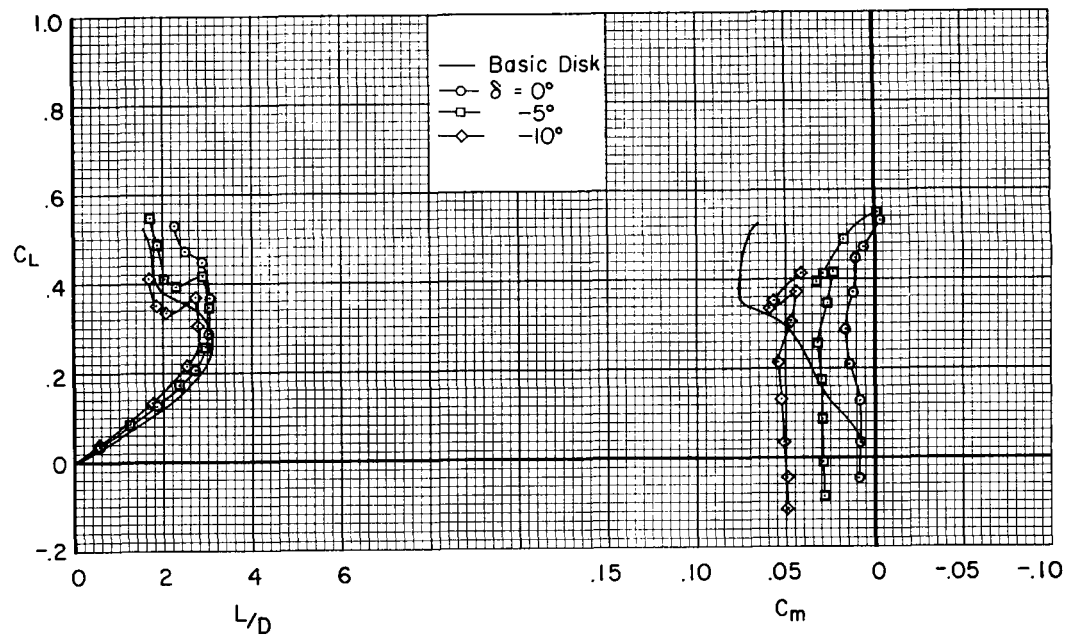

(d) M = 0.90

Figure 9.- Concluded.

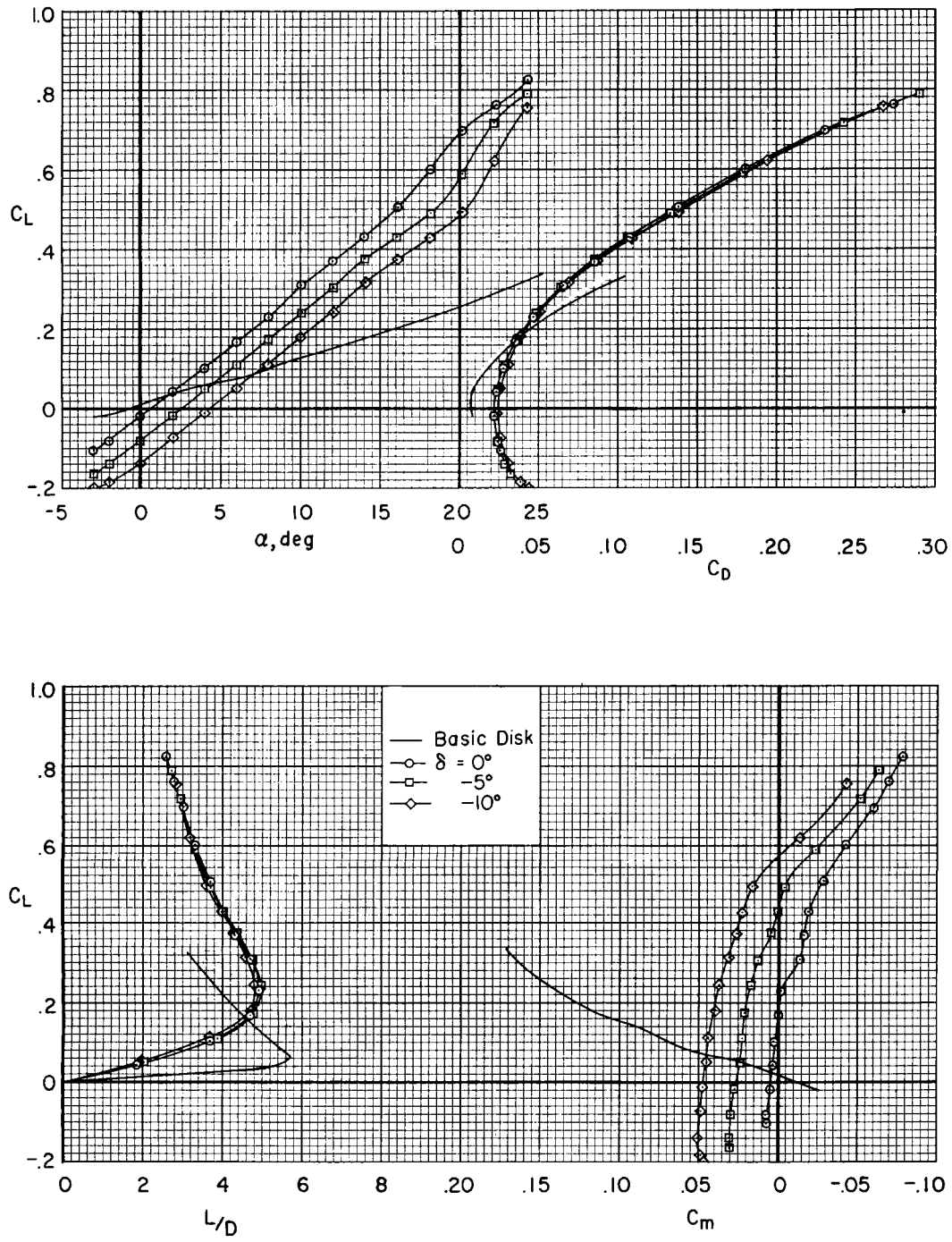

(a) $R = 3.3 \times 10^6$

Figure 10.- The longitudinal aerodynamic characteristics of the model and basic disk having a thickness-diameter ratio of 0.325; 25-percent flaps; small canopy; vertical surfaces on; M = 0.25.

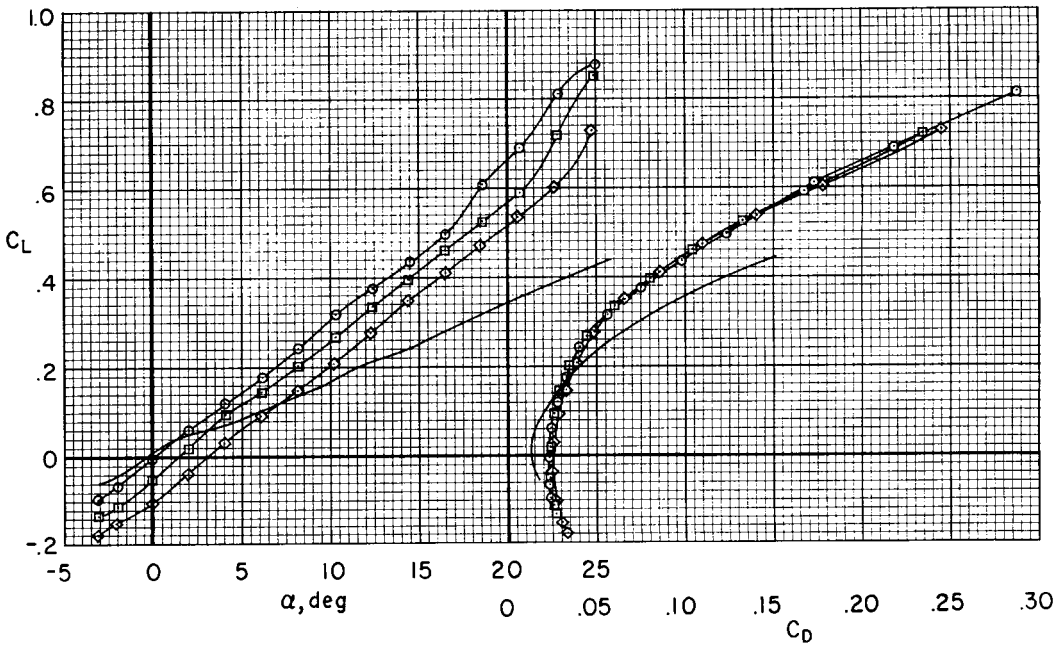

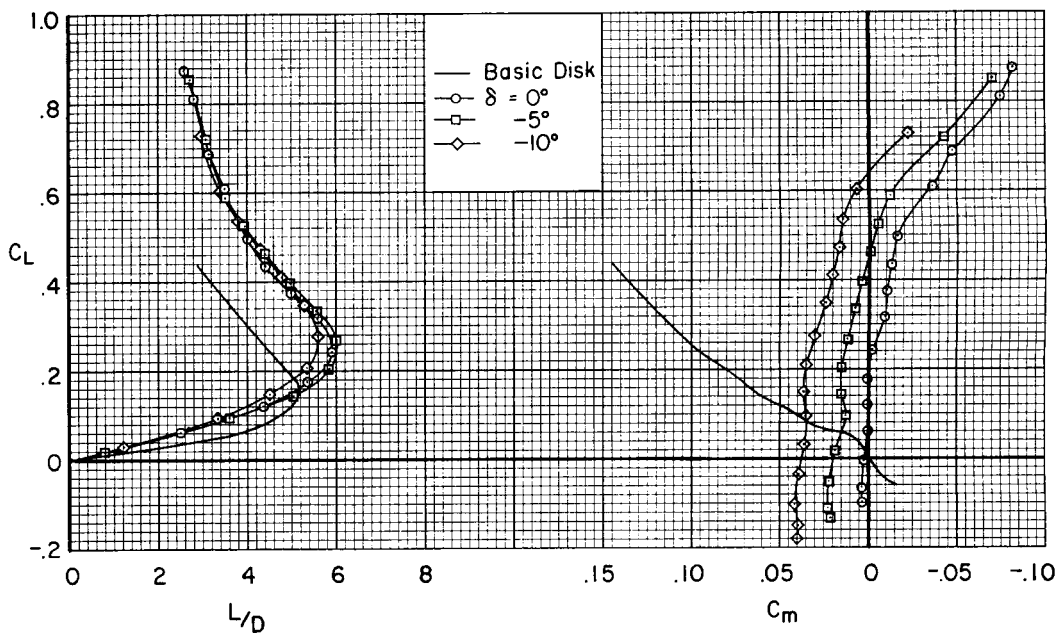

(b) R = 16×10^6

Figure 10.- Concluded.

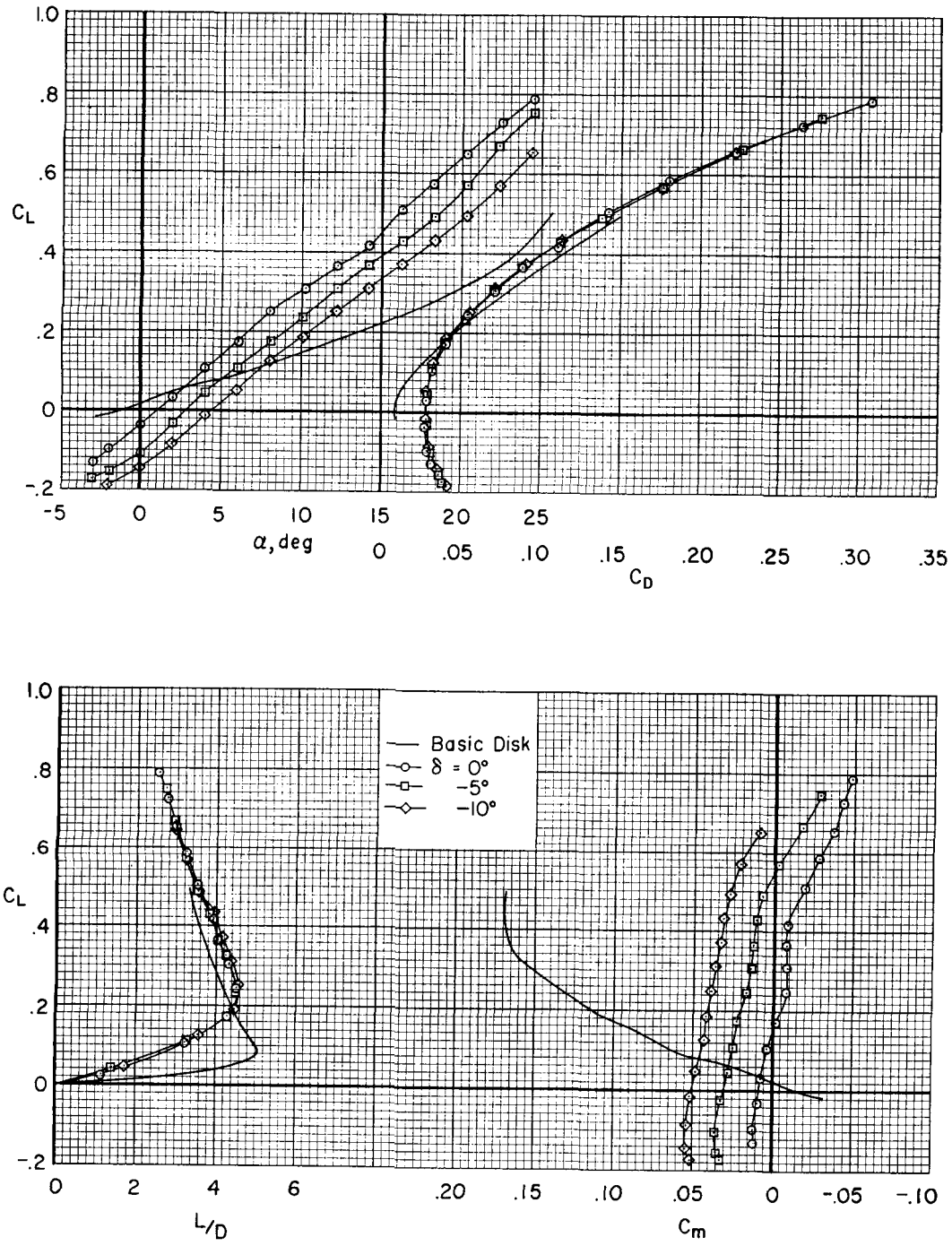

(a) M = 0.60

Figure 11.- The longitudinal aerodynamic characteristics of the model and basic disk having a thickness-diameter ratio of 0.325; 25-percent flaps; small canopy; vertical surfaces on; $R = 3.3 \times 10^6$.

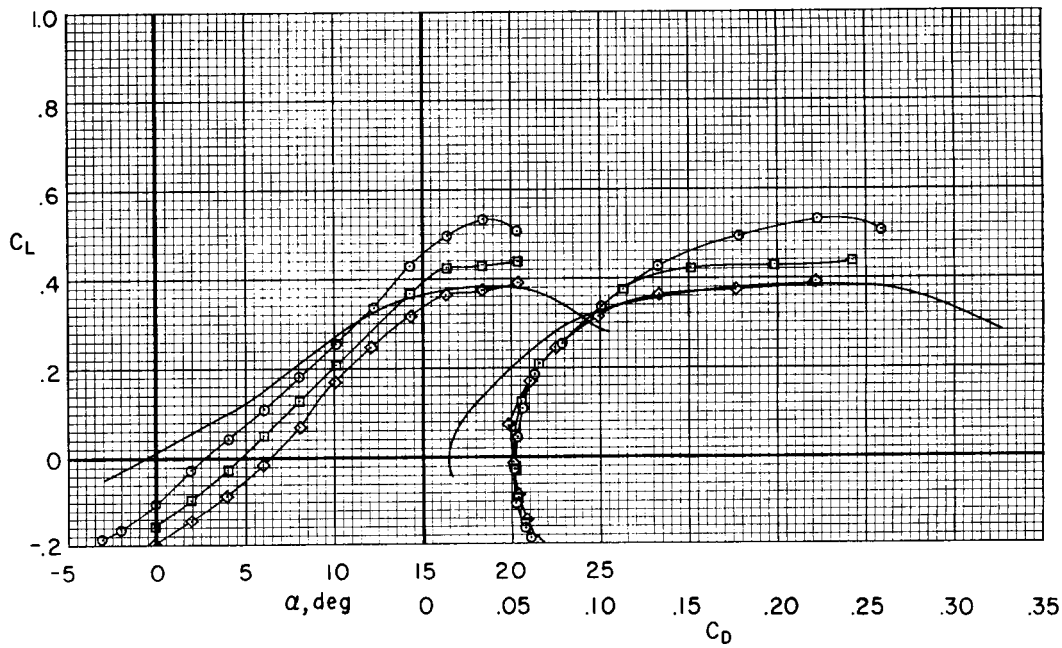

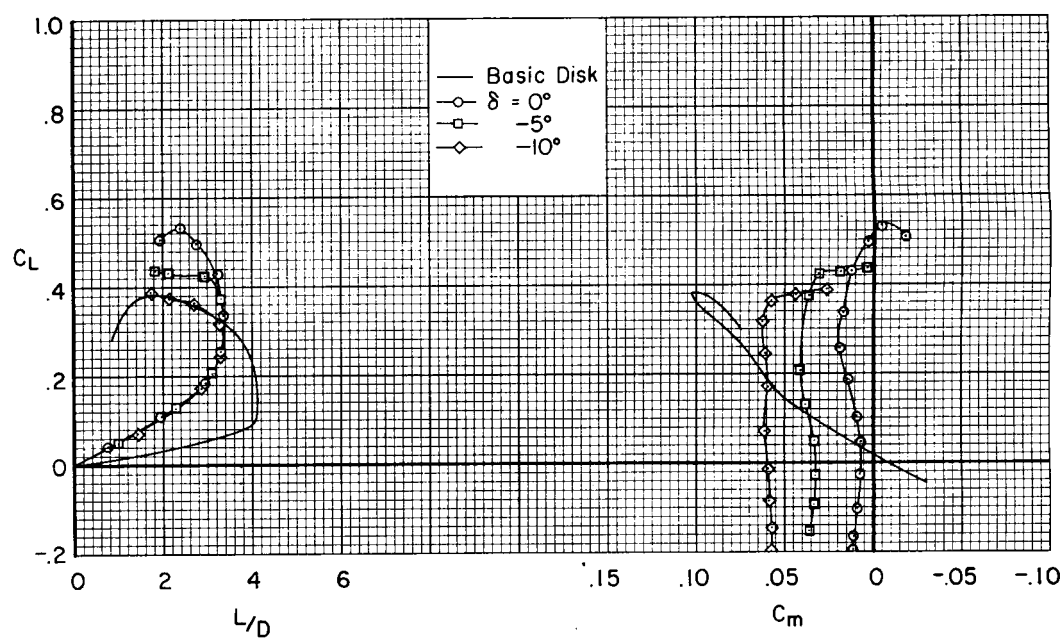

(b) M = 0.80

Figure 11.- Continued.

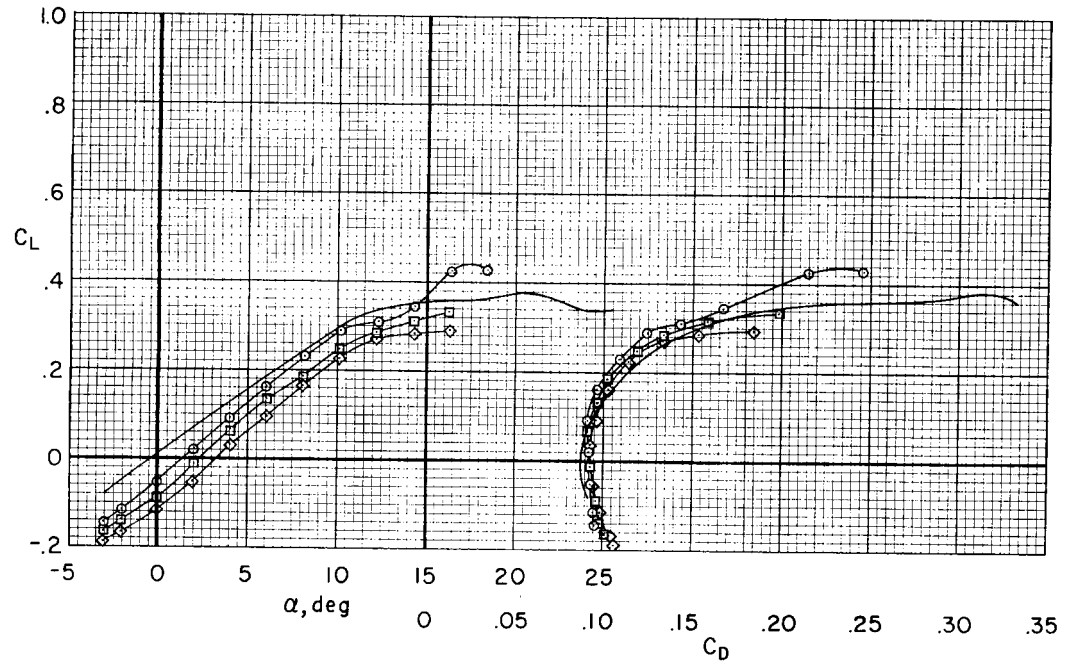

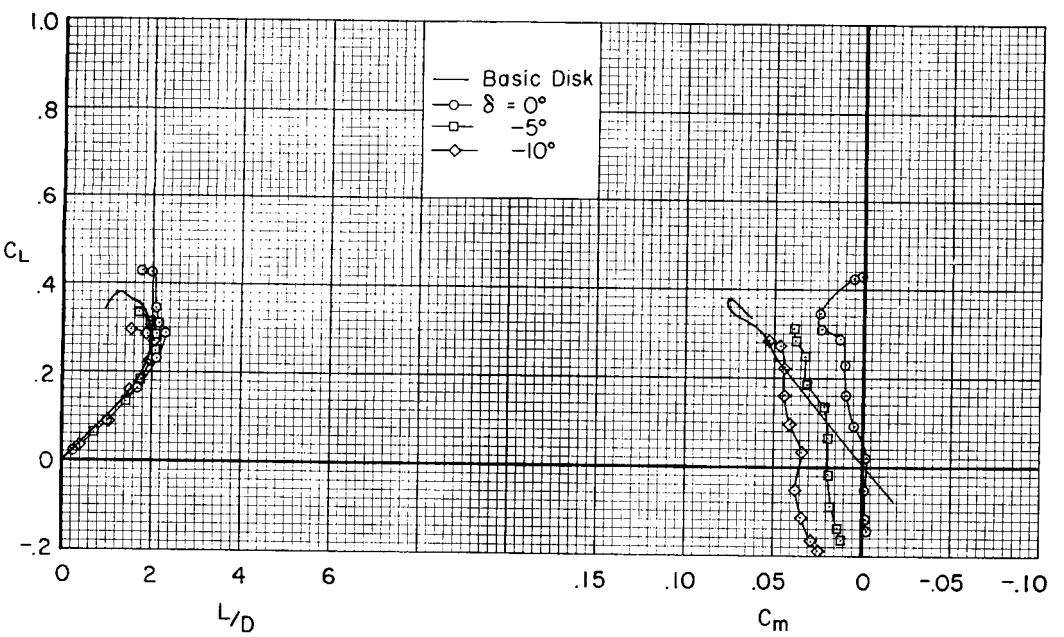

(c) M = 0.85

Figure 11.- Continued.

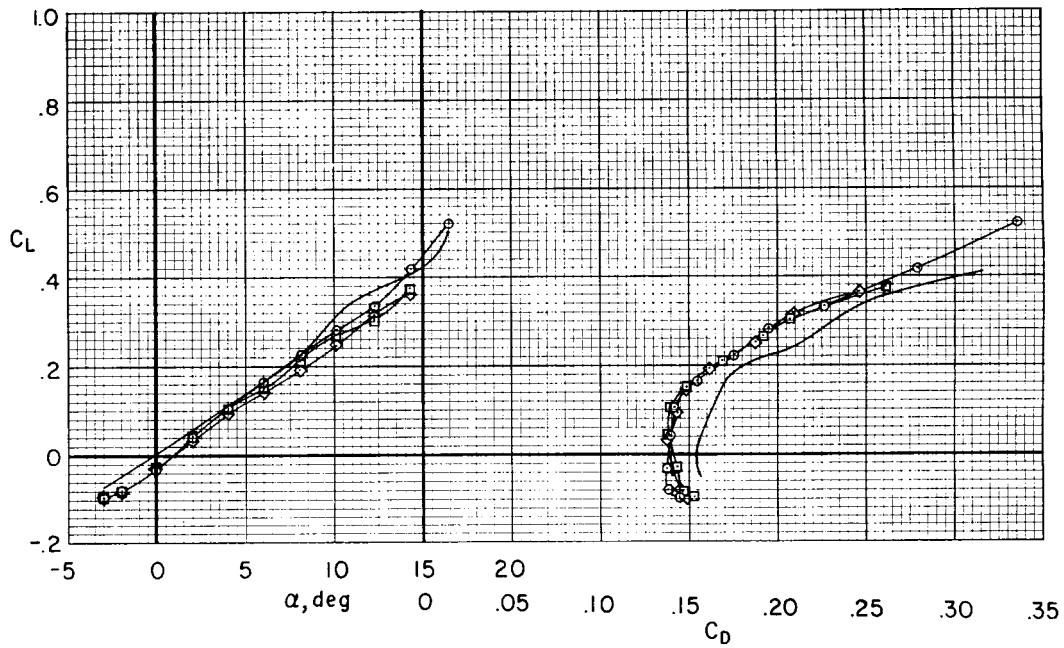

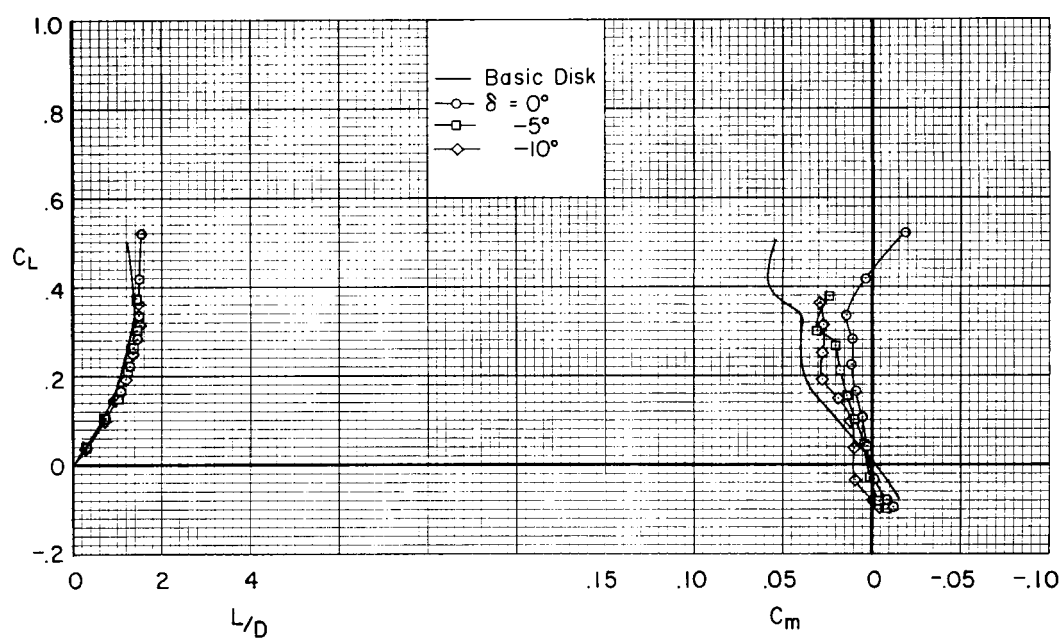

(d) M = 0.90

Figure 11.- Concluded.

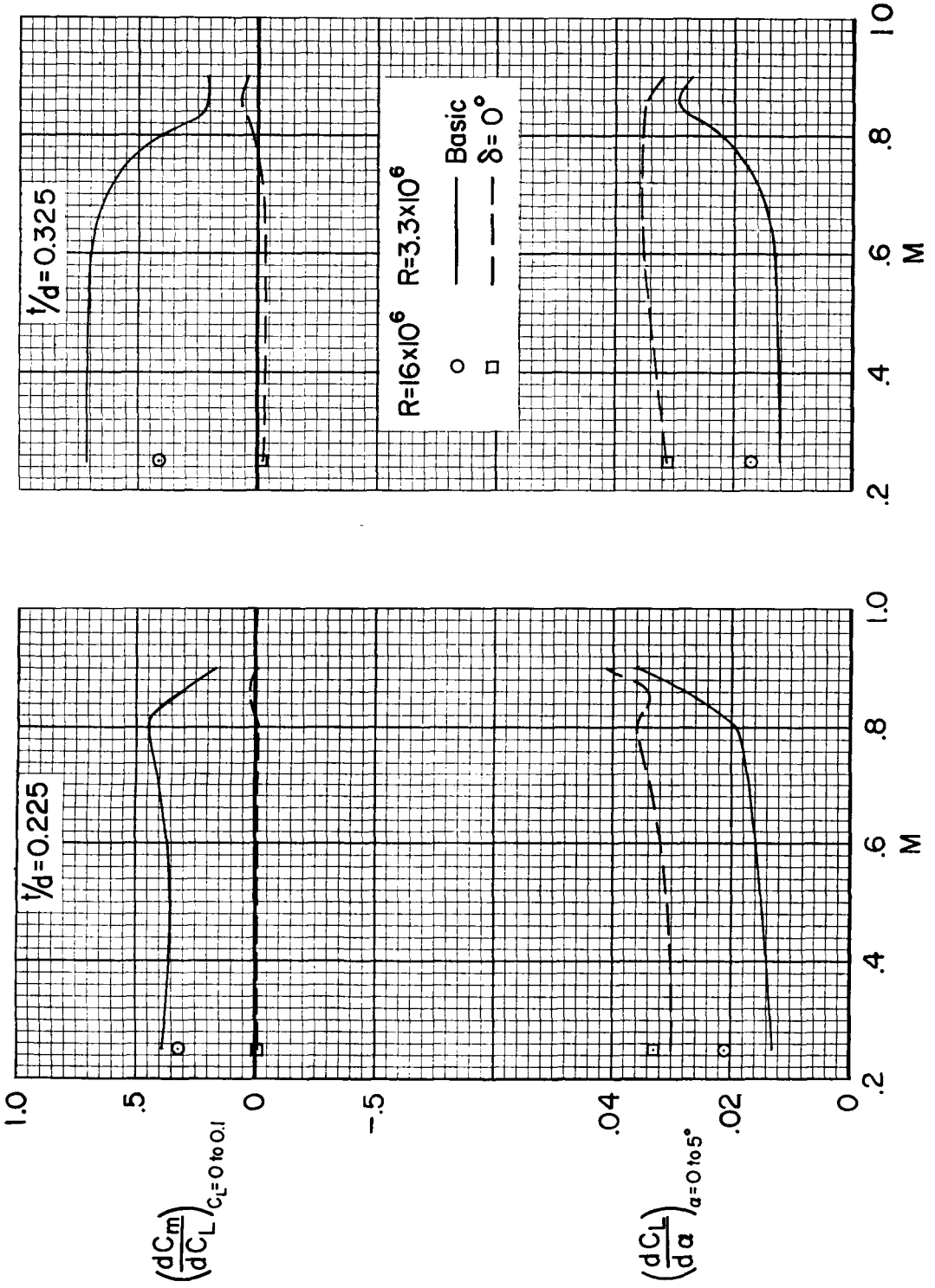

Figure 12.- The variation with Mach number of lift- and pitching-moment-curve slopes for the model configurations and basic disk shapes.

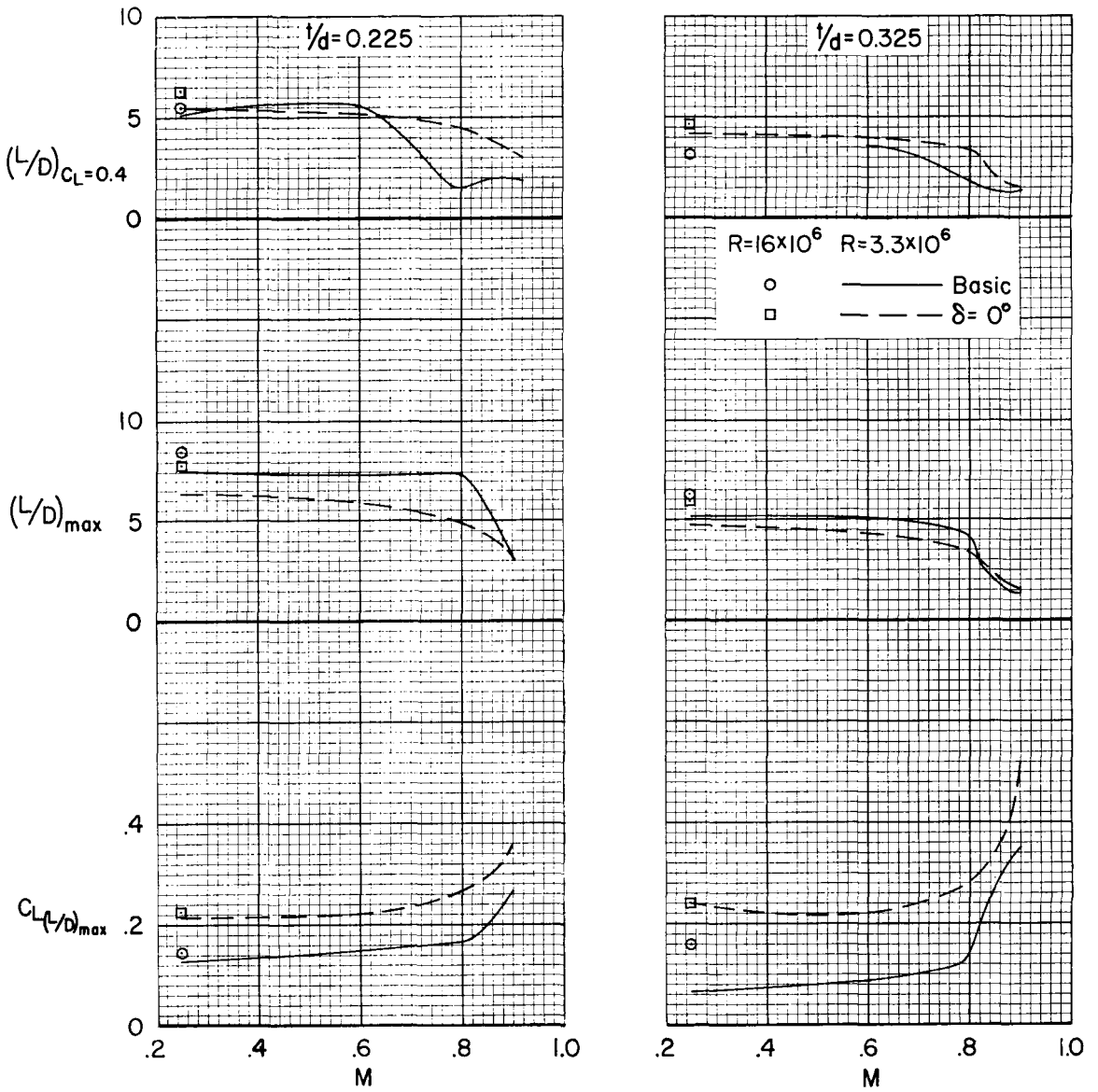

Figure 13.- The variation with Mach number of lift-drag characteristics for the model configurations and basic disk shapes.

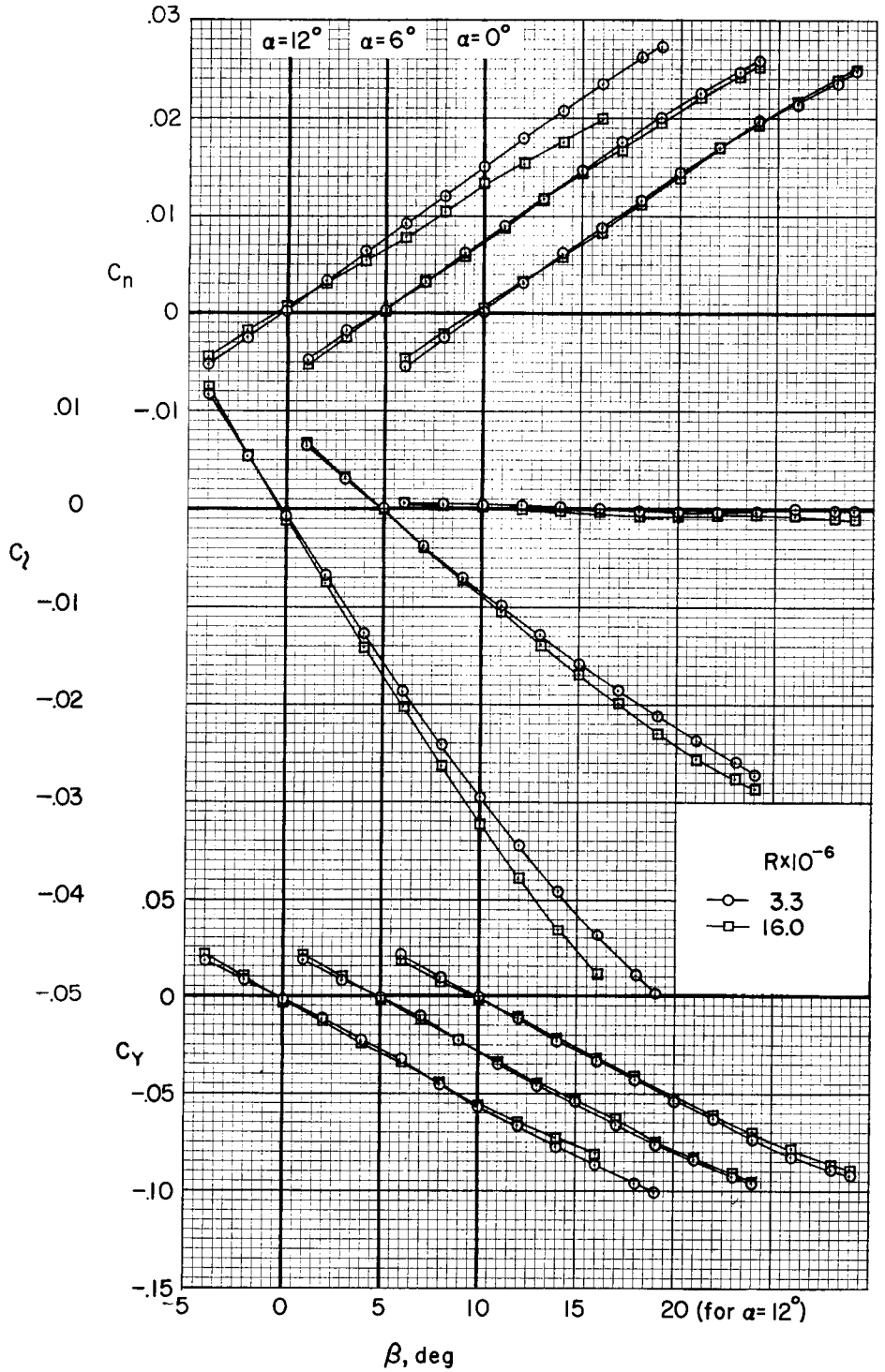

Figure 14.- The effect of Reynolds number on the lateral characteristics of the model having a thickness-diameter ratio of 0.225; 20-percent flaps; $\delta = 0^\circ$; small canopy; vertical surfaces on; M = 0.25.

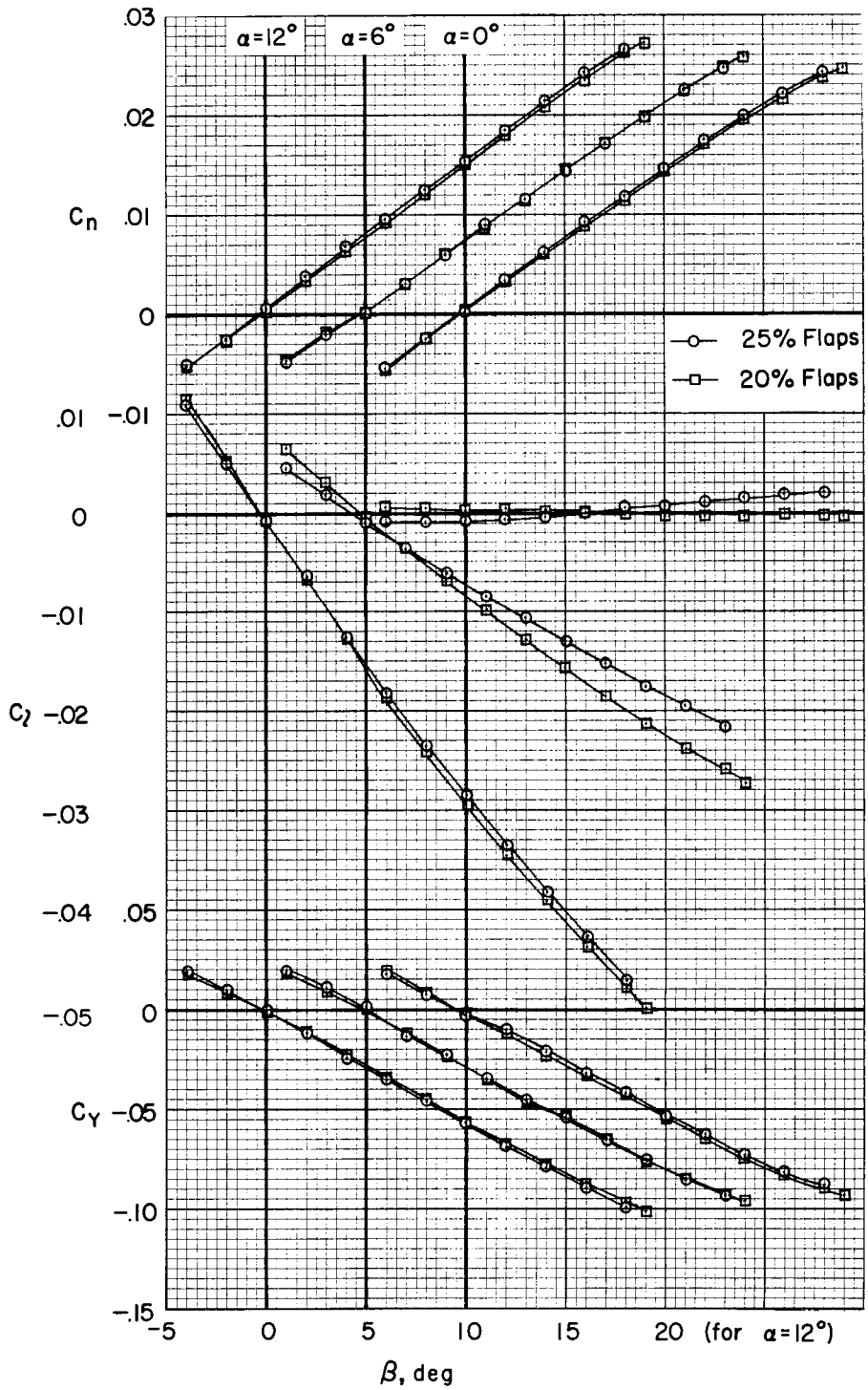

Figure 15.- The effect of flap size on the lateral characteristics of the model having a thickness-diameter ratio of 0.225; $\delta = 0^{\circ}$; small canopy; vertical surfaces on; M = 0.25; R = 3.3×10^{6}.

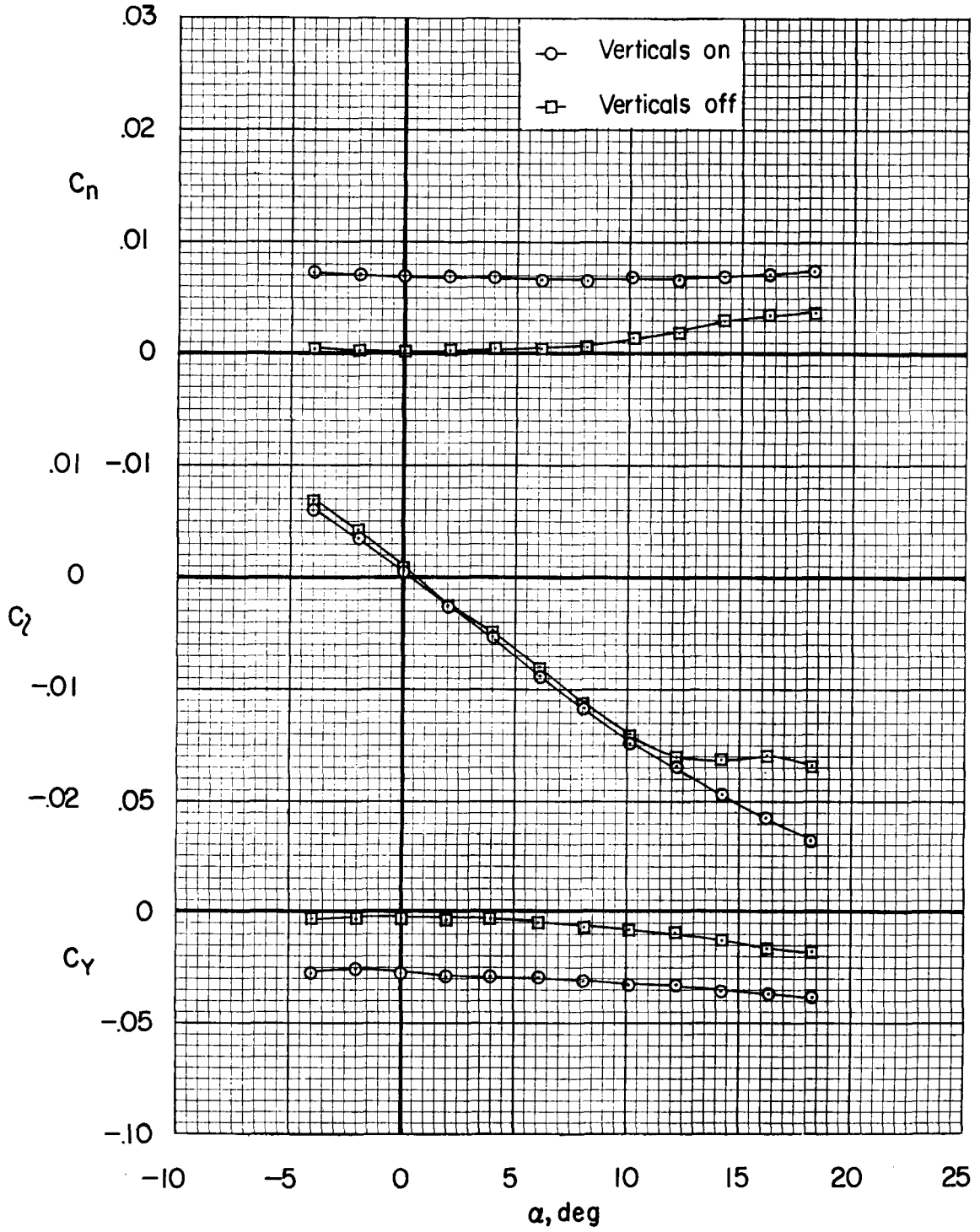

Figure 16.- The variation with angle of attack of the lateral characteristics of the model having a thickness-diameter ratio of 0.225; 25-percent flaps; $\delta = 0^{\circ}$; small canopy; $\beta = 6^{\circ}$; $M = 0.25$; $R = 3.3 \times 10^{6}$.

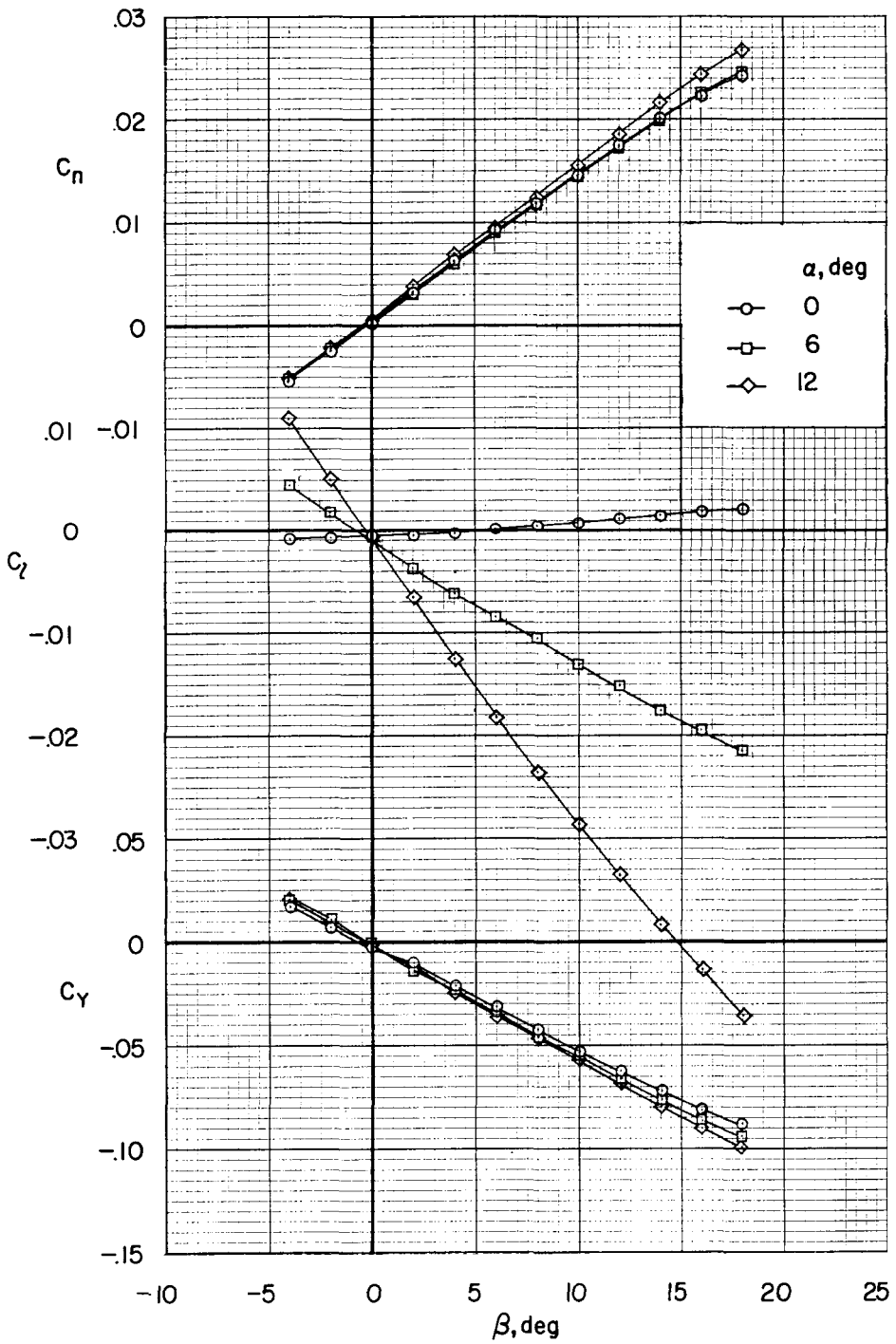

(a) M = 0.25

Figure 17.- The lateral characteristics of the model having a thickness-diameter ratio of 0.225; 25-percent flaps; $\delta = 0^{\circ}$; small canopy; vertical surfaces on; $R = 3.3 \times 10^{6}$.

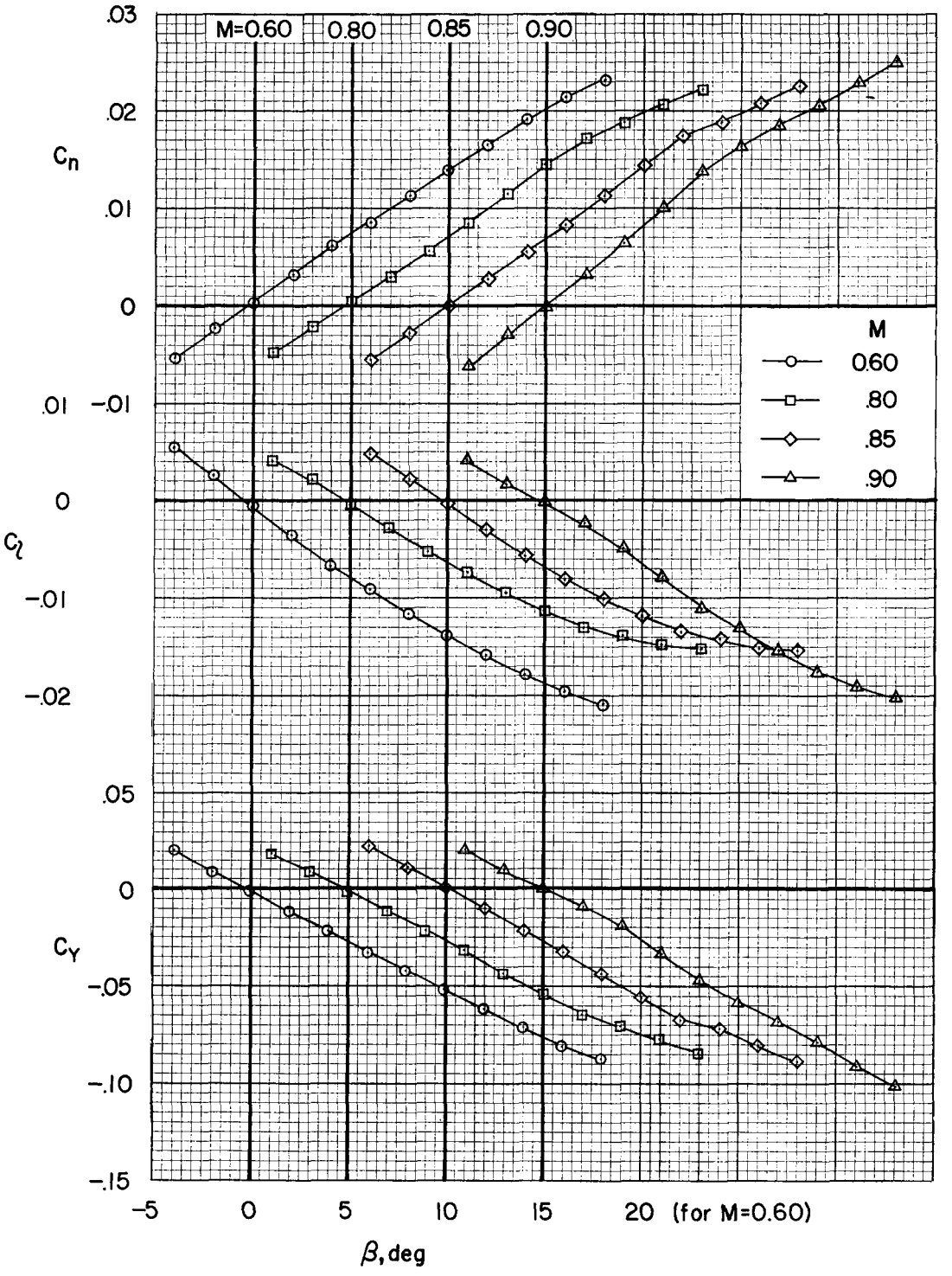

(b) M = 0.60 to 0.90; $\alpha = 6^\circ$

Figure 17.- Concluded.

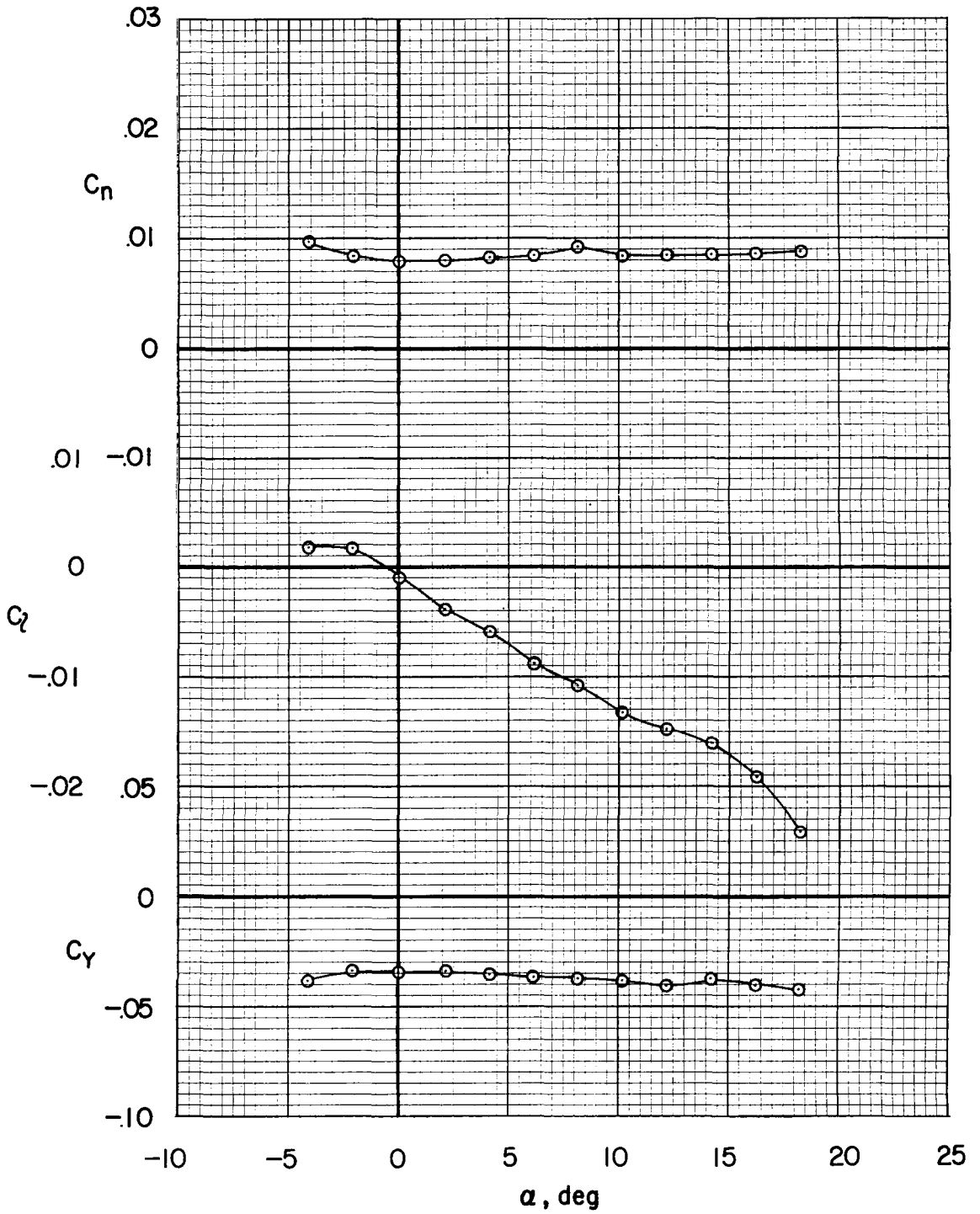

Figure 18.- The variation with angle of attack of the lateral characteristics of the model having a thickness-diameter ratio of 0.325; 25-percent flaps; $\delta = 0^{\circ}$; $\beta = 6^{\circ}$; small canopy; vertical surfaces on $M = 0.25$; $R = 3.3 \times 10^{6}$.

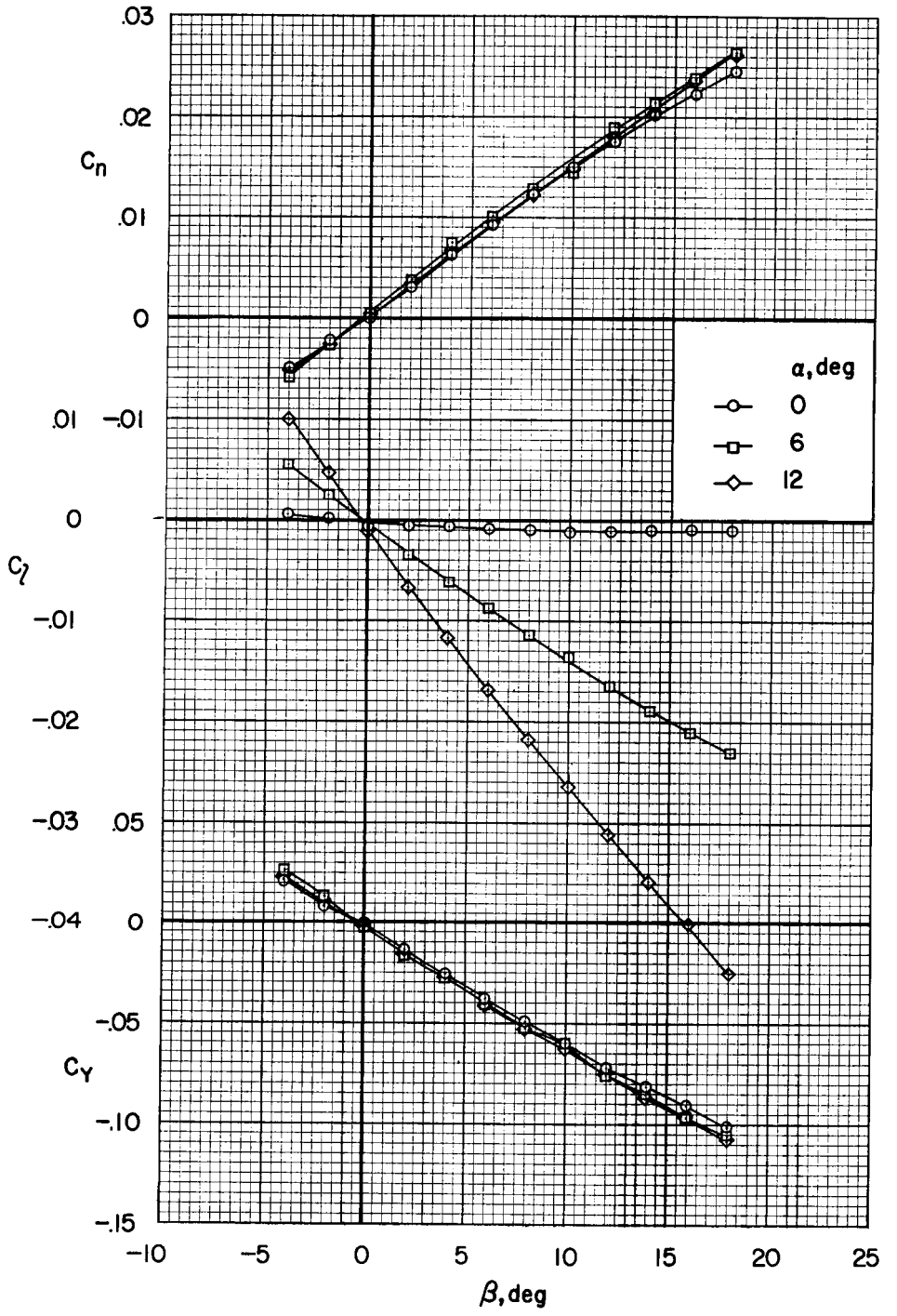

(a) M = 0.25

Figure 19.- The lateral characteristics of the model having a thickness-diameter ratio of 0.325; 25-percent flaps; $\delta = 0^{\circ}$; small canopy; vertical surfaces on; $R = 3.3 \times 10^{6}$.

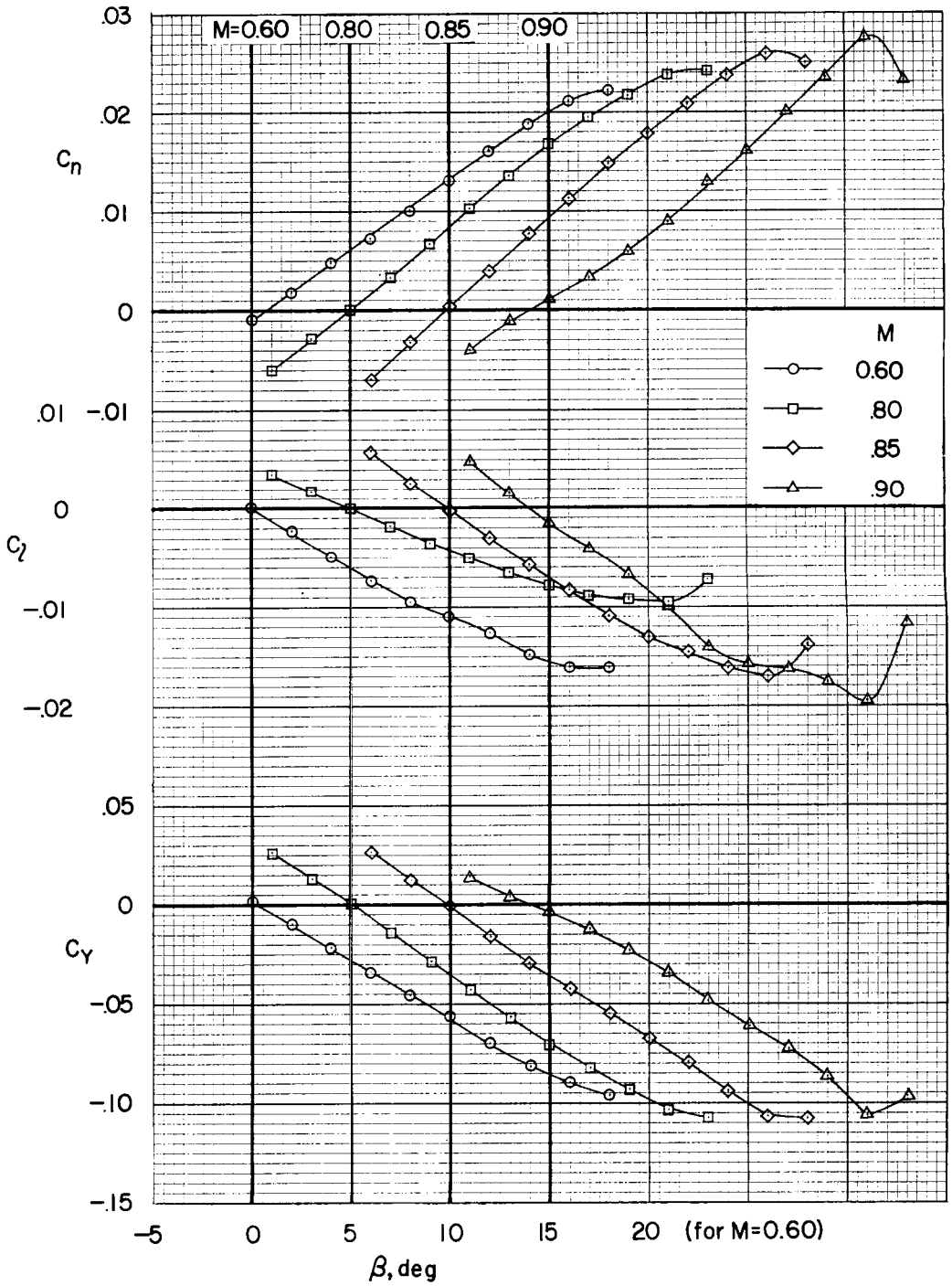

(b) M = 0.60 to 0.90; $\alpha = 6^\circ$

Figure 19.- Concluded.

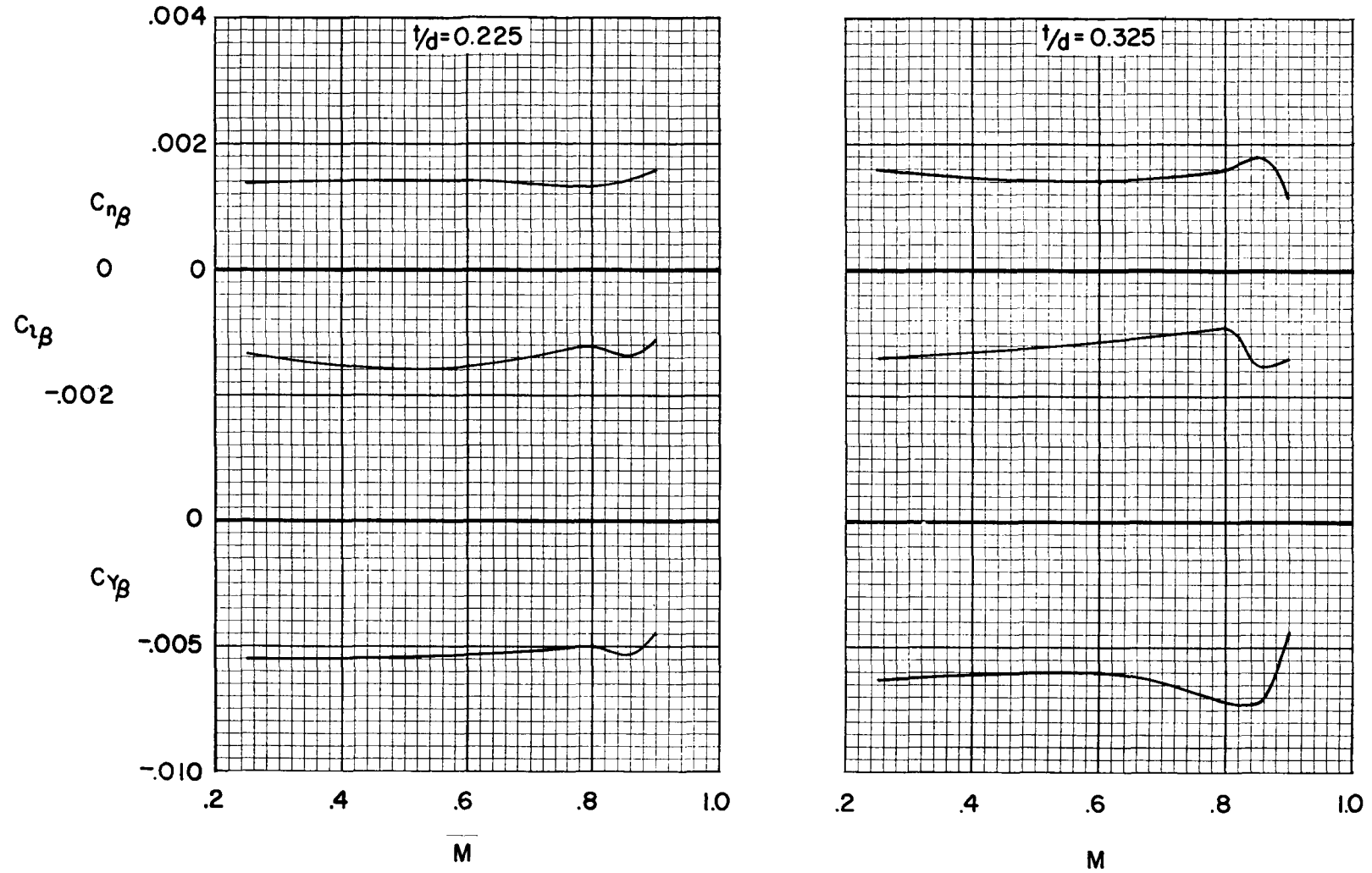

Figure 20.- The variation with Mach number of the lateral stability derivatives; 25-percent flaps; $\delta = 0^\circ$; small canopy; vertical surfaces on; $\alpha = 6^\circ$; $R = 3.3 \times 10^6$.

UNCLASSIFIED